HORIZONTAL AND SLANTED WELLS IN LAYERED RESERVOIRS WITH CROSSFLOW

A REPORT
SUBMITTED TO THE DEPARTMENT OF PETROLEUM ENGINEERING
OF STANFORD UNIVERSITY
IN PARTIAL FULFILLMENT OF THE REQUIREMENTS
FOR THE DEGREE OF
MASTER OF SCIENCE

By
Pengbo Lu
June 1997

I certify that I have read this report and that in my opinion it is fully adequate, in scope and in quality, as partial fulfillment of the degree of Master of Science in Petroleum Engineering.

Roland N. Horne
(Principal advisor)

Acknowledgements

I would like to thank my advisor Professor Roland N. Horne for his advice, guidance, and encouragement during the course of this research. Sincere thanks are due to Dennis Gommard for unselfishly providing his report and programming codes for this research. My girl friend, Jing Wan, also my colleague, always gives me her wholehearted support and help. My gratitude to her is beyond description. I also wish to express my appreciation to my friends and colleagues, Suwat Athichanagorn, Antonio Bittencourt, Jorge Landa and Yan Pan for generously providing good ideas and techniques for this research.

Financial support from Stanford University Petroleum Research Institute (SUPRI-D) and the Department of Petroleum Engineering are gratefully acknowledged.

I would like to thank my family for their love and support. My special gratitude is endless to my parents, Zhijian Lu and Huaiyun Wang, and to my brother Zhaohui Lu.

Abstract

The purpose of this report is to present new analytical pressure-transient solutions for horizontal and slanted wells in layered reservoirs with crossflow. We considered two different situations: (1) the pressure-transient behavior of a single slanted well crossing several layers; (2) interference between several horizontal wells located at different positions. These layered systems can be bounded by two horizontal impermeable boundary planes at the top and the bottom, or either one of the boundary planes can be a constant-pressure boundary (the system either has a gas cap or an active aquifer).

We used the Laplace transform and double Fourier cosine transform to obtain the Green's functions for the layered and composite systems. For this type of problem, it is convenient to express the Green's function as the sum of two solutions: the point source solution and the solution of the homogeneous partial differential equation for each layer. The point source solution can be obtained in the Laplace space. However, due to the complication of the crossflow interfaces, we applied double Fourier cosine transform and obtained the solution of the homogeneous partial differential equation. The reflection and transmission method was introduced to solve the layered and composite systems, which can not be solved by the conventional methods.

The segmentation method was used to solve the pressure transient behavior. The wellbore was discretized into several segments and each segment was treated as uniform flux, then we set up a linear system and obtained the pressure drop solution in the Laplace space and transformed it back to the real space.

Contents

List of Tables

List of Figures

Section 1

Introduction

Productivity improvement and acceleration projects have gained substantially from the success of horizontal well drilling technology. The successful placement of near-horizontal wells in difficult reservoir configurations has become routine. Therefore, determination of transient pressure behavior for horizontal wells has aroused considerable interest over the past decade. Articles on horizontal wells are too numerous to cite. An extensive literature survey on horizontal wells can be found in Refs. [1][2]. Most of these papers dealt with horizontal wells only in a single, homogeneous layer[3]–[8].

Recently, a number of papers have also considered horizontal wells in multilayered reservoirs. Spath, *et al.*,[9] described an efficient algorithm for computation of pressure transient solutions in commingled reservoirs, which took advantage of a unique feature of commingled-reservoir production (layer rates are independent of each other because the system is decoupled) for the constant-terminal-pressure solution. However, this algorithm can not deal with crossflow between layers. Kuchuk[10][11] presented a new general method for solving transient pressure problems in lateral composite reservoirs. In these composite systems, the properties of facies change laterally. Kuchuk also showed new analytical solutions for horizontal wells with wellbore storage and skin in layered reservoirs with crossflow. This method was based on the principles of reflection and transmission. It is shown that a network of partially communicating faults and fractures in porous medium can be modeled as composite systems.

However, not all reservoir situations are appropriate for horizontal drilling. Specifically, laminated reservoirs with very small vertical permeability, i.e., $k_v/k_h \approx 0$, have been perceived as poor targets. Potentially large reserves are locked in these reservoirs. In general, a small well count is essential to help minimize development costs. To achieve requirements of both high productivity and small well count, slanted wells ($0^o \leq \theta_w \leq 10^o$) cutting the entire sand package are desirable. Such well configurations have been known to improve productivity of these wells.

Roemershauser and Hawkins[12] studied steady state flow in a reservoir producing through a fully-slanted well by using an electrical model. They considered a circular reservoir of finite extent and concluded that the slant of a fully-penetrating well causes an increase in the resistance to flow around the well due to the increase in the producing interval area exposed to flow. Cinco[13][14] investigated the same kind of problem using the Green's functions. He considered a slanted well in an infinite slab reservoir and obtained the analytical solution in two ways: a) by integrating a point source solution along a segment considering the flow uniform in the well; b) representing the well as an infinite conductivity source so that the pressure transient is the same along the well. Cinco studied the influence of the non-uniformity of the flow-rate distribution along the source, and showed that the average pressure at the wellbore give a good approximation to the infinite conductivity wellbore pressure for a slanted well and defined an equivalent point which the pressure matches the average pressure.

Fair *et al.*[15] showed that the deviated well model given by Cinco fails to predict any improvement in well productivity. Bed thickness, well diameter, and well angle control the productivity of these thin-bedded sequences. In Fair's paper, a simple technique to calculate the productivity improvement factor (PIF) is derived for wells that are nearly horizontal. The range of validity of this approximation was determined by comparison with fine-grid simulations. This model is restricted to cases in which the bed is thin so that flow is horizontal into wellbore. In thin beds completed with a deviated wellbore, the flow near the wellbore may have a significant vertical component. Cinco's solution handles this correctly for wells with $\theta_w > 15^o$; however,

all the flow is horizontal as beds become thin.

Some papers also studied the productivity index of an inclined well in finite-difference reservoir simulation. Lee and Milliken[16] showed the method of reflections and slender body theory to provide a means to obtain accurate measures of the productivity index in complex reservoir formations. Using slender body theory, Lee and Milliken derived an asymptotic solution of single-phase flow around an inclined well, this solution was applied to determine the productivity index. The method of reflections can account for the presence of layer boundaries through the application of image solutions. In combination, these techniques permit the calculation of the productivity index in anisotropic formations with layer boundaries.

Gommard[17] investigated almost horizontal wells in multilayered reservoirs with crossflow. He studied the segmentation technique to obtain an optimum subdivision to calculate the pressure drop response of a well with either infinite conductivity or uniform flow-rate distribution. He showed that the infinite conductivity solution, the equivalent pressure point solution and the averaged pressure drop solution tended to give different responses in early times (after the first radial flow period). He also developed an analytical solution to calculate the averaged pressure drop for a well in a multilayered reservoir, which can decrease the computation time significantly. However, he did not include a solution for slanted wells crossing several layers.

This study was based on Kuchuk's[10] and Gommard's[17] works and concentrates on the pressure transient behavior of slanted wells ($0^o \leq \theta_w \leq 10^o$) crossing several layers in multilayered reservoirs with crossflow. The interference between several horizontal wells in such kind of reservoirs was also investigated.

Section 2

Governing Equations and Coordinate System

2.1 Governing Equations

Let us consider an infinite anisotropic layered medium bounded by the top and the bottom boundary planes, which are either no-flow, constant-pressure or infinite acting. All the layers are horizontal layers with crossflow. The boundary conditions in the z direction are either no-flow, constant-pressure or infinite acting. The permeabilities of each layer in the principal directions are denoted by $(k_x)_i$, $(k_y)_i$ and $(k_z)_i$. The configuration of the layered reservoir is shown in Fig. 2.1. The flow of a slightly compressible fluid of constant compressibility and viscosity is assumed for each layer.

The pressure diffusion equation for the i-th layer is given by

$$(k_x)_i \frac{\partial^2 p_i}{\partial x^2} + (k_y)_i \frac{\partial^2 p_i}{\partial y^2} + (k_z)_i \frac{\partial^2 p_i}{\partial z^2} = (\phi \mu c_t)_i \frac{\partial p_i}{\partial t}. \tag{2.1}$$

The boundary conditions at the top (first layer) and bottom (n-th layer) are:

$$\gamma_i p_i(\mathbf{r}, t) + \zeta_i \frac{\partial p_i}{\partial z}(\mathbf{r}, t) = 0; \text{ at } z_1 = h_1 \text{ and } z_n = 0, \tag{2.2}$$

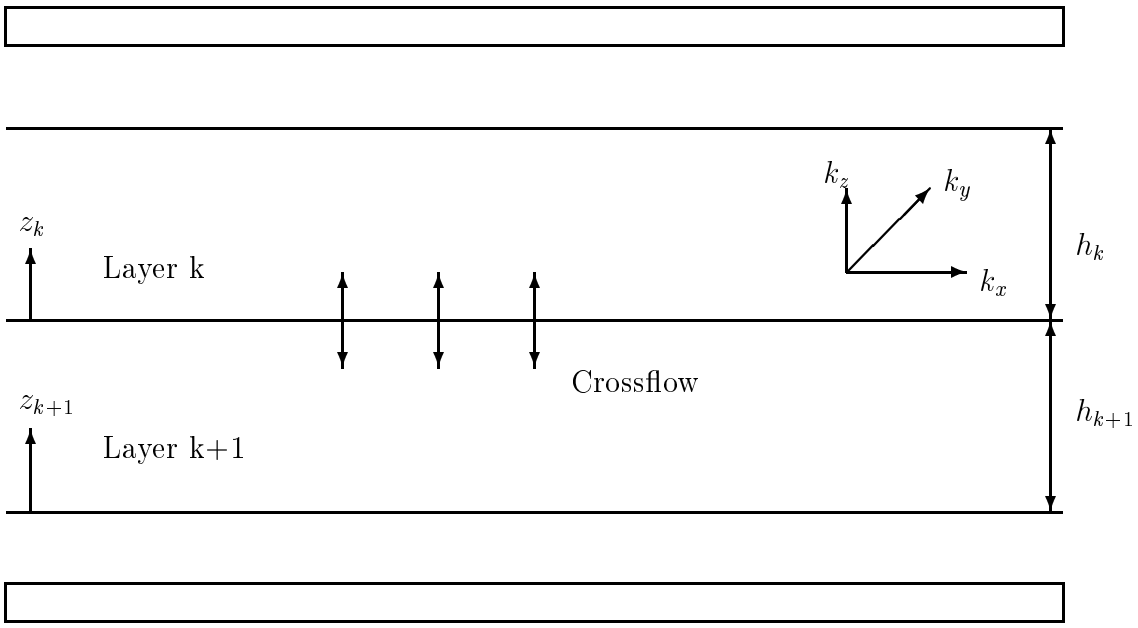

Figure 2.1: Configuration of a Layered Reservoir

where $\mathbf{r}(x, y, z)$ is the three-dimensional position vector, h_i is the thickness of the i-th layer and z_i is the z-coordinate in a local coordinate system, in which the origin of the z-coordinate is assumed to be the interface of two adjacent layers. In the formation, one layer is chosen as the *reference layer, Layer r*. For a suitable choice of γ and ζ on the boundaries, Eqn. 2.2 can represent no-flow ($\gamma = 0$, $\zeta = 1$) or constant-pressure ($\gamma = 1$, $\zeta = 0$) boundary condition.

The boundary condition in the $x - y$ plane is

$$p_i(\mathbf{r}, t) = p_0 \text{ as x and } y \to \infty. \tag{2.3}$$

The initial condition is

$$p_i(\mathbf{r}, 0) = p_0 \text{ at } t = 0. \tag{2.4}$$

In our approach, the individual well segment was treated as a uniform-flux source.

Thus the inner boundary condition for the i-th segment is

$$\lim_{\mathbf{r}\to 0} \zeta_i \frac{\partial p}{\partial n} = \begin{cases} 0; & \text{not on Segment } i; \\ q_i(t); & \text{on Segment } i \end{cases}, \tag{2.5}$$

where $\frac{\partial}{\partial n}$ is the conormal derivative and ζ_i is a constant in each layer.

The continuity conditions at the layer interfaces are:

$$p_i(\mathbf{r}, t) = p_{i+1}(\mathbf{r}, t) \text{ at z } = z_i, \tag{2.6}$$

and

$$(\frac{k_z}{\mu})_i \frac{\partial p_i}{\partial z}(\mathbf{r}, t) = (\frac{k_z}{\mu})_{i+1} \frac{\partial p_{i+1}}{\partial z}(\mathbf{r}, t) \text{ at z } = z_i. \tag{2.7}$$

2.2 Dimensionless Parameters and Equations

In this paper, all the parameters are defined in field units. Thus dimensionless time and pressure are defined as

$$t_D = \frac{0.0002637(k_x)_r t}{(\phi \mu c_t)_r L_w^2}, \tag{2.8}$$

and

$$(p_D)_i = \frac{2\sqrt{(k_y)_r (k_z)_r} L_w}{141.2 q \mu_r} [p_0 - (p_w)_i(t)], \tag{2.9}$$

and other dimensionless parameters as

$$(h_D)_i = \frac{h_i}{L_w}, \tag{2.10}$$

$$x_D = \frac{x}{L_w}, \tag{2.11}$$

$$y_D = \frac{y}{L_w}, \tag{2.12}$$

$$z_D = \frac{z}{L_w}, \tag{2.13}$$

$$z_{wD} = \frac{z_w}{L_w}. \tag{2.14}$$

The effective dimensionless wellbore radius is

$$r_{wD} = \frac{r_w}{2L_w} \left\{ \sqrt{(\frac{k_x}{k_y})_i} + \sqrt{(\frac{k_x}{k_z \cos^2\theta_w + k_x \sin^2\theta_w})_i} \right\}, \tag{2.15}$$

where the subscript r denotes the properties of the referred layer, and i denotes properties of the i-th layer, and θ_w is the deviation angle from the horizontal direction.

Substitution of these variables in Eqn. 2.10-2.14 gives

$$\frac{\partial^2 p_{Di}}{\partial x_D^2} + (\lambda_y)_i \frac{\partial^2 p_{Di}}{\partial y_D^2} + (\lambda_z)_i \frac{\partial^2 p_{Di}}{\partial z_D^2} = \frac{1}{\kappa_i} \frac{\partial p_{Di}}{\partial t_D}, \tag{2.16}$$

where

$$(\lambda_y)_i = (\frac{k_y}{k_x})_i, \tag{2.17}$$

$$(\lambda_z)_i = (\frac{k_z}{k_x})_i, \tag{2.18}$$

$$\kappa_i = \frac{\eta_i}{\eta_r}, \tag{2.19}$$

$$\eta_i = (\frac{k_x}{\phi \mu c_t})_i. \tag{2.20}$$

Then Eqn. 2.15 can be rewritten as

$$r_{wD} = \frac{r_w}{2L_w} \left\{ \frac{1}{\sqrt{(\lambda_y)_i}} + \frac{1}{\sqrt{(\lambda_y)_i \sin^2 \theta_w + \cos^2 \theta_w}} \right\}. \tag{2.21}$$

2.3 Governing Equations in the Laplace Domain

In the Laplace domain, the diffusion equation given by Eq. 2.16 with its initial condition becomes

$$\frac{\partial^2 \bar{p}_{Di}}{\partial x_D^2} + (\lambda_y)_i \frac{\partial^2 \bar{p}_{Di}}{\partial y_D^2} + (\lambda_z)_i \frac{\partial^2 \bar{p}_{Di}}{\partial z_D^2} - \frac{s}{\kappa_i} \bar{p}_{Di} = 0. \tag{2.22}$$

This is the three-dimensional Helmholtz equation for the diffusivity equation, where $\bar{p}_{Di}$ is real and the frequency variable $-\frac{s}{\kappa_i}$ is negative. Normally, for the Helmholtz equation, the frequency variable is non-negative. We will discuss the Green's function method applicable to this type of equation in next chapter.

Section 3

Fundamental Green's Function Solutions

3.1 Green's Function Method

3.1.1 Basic Concept and Green's Theorem

The general form of a partial differential equation is given as

$$\mathcal{L}u(\mathbf{r}) = \phi(\mathbf{r}) \text{ defined in the domain } \Omega \ , \tag{3.1}$$

with boundary conditions on the boundary Γ, where $\mathcal{L}$ is a differential operator.

Now let us integrate the product vDu by parts over the domain Ω of interest repeatedly. The result can be expressed as

$$\iint_\Omega v\mathcal{L}u d\Omega = \oint_\Gamma [\cdots] d\Gamma + \iint_\Omega u\mathcal{L}^* v d\Omega, \tag{3.2}$$

where $[\cdots]$ denotes an expression to be integrated along Γ, $\mathcal{L}^*$ is the adjoint operator of $\mathcal{L}$, and the functions u and v are arbitrary as long as they are differentiable for the operator $\mathcal{L}$.

In some cases, $\mathcal{L}^* = \mathcal{L}$, the operator $\mathcal{L}$ is said to be *self-adjoint*. For example, Green's theorem (second formula) gives

$$\iint_\Omega v\nabla^2 u d\Omega = \oint_\Gamma (v\frac{\partial u}{\partial n} - u\frac{\partial v}{\partial n}) d\Gamma + \iint_\Omega u\nabla^2 v d\Omega, \tag{3.3}$$

so the Laplace operator ∇^2 is self-adjoint.

The modified Helmholtz operator $H = \nabla^2 - \lambda$ with λ real and positive is also self-adjoint according to the second formula of Green's theorem. Therefore we can have

$$\iint_\Omega vHud\Omega = \oint_\Gamma (v\frac{\partial u}{\partial n} - u\frac{\partial v}{\partial n})d\Gamma + \iint_\Omega uHvd\Omega. \tag{3.4}$$

The integral of the form $v(\partial u/\partial n) - u(\partial v/\partial n)$ is crucial in the Green's function method. In boundary-value problems in terms of u, the boundary conditions are usually prescribed in terms of u and/or $\partial u/\partial n$, and, hence, if the function v can be determined such that it cancels unprescribed boundary conditions and such that the double integral terms are reduced to simpler forms, the resultant equation becomes solvable for u. Unfortunately, most partial differential equations do not give the integrand form desirable in the Green's function method. However, some partial differential equations can be written in forms which can be solved using the Green's function method with some simple boundary conditions. In next section, we discuss the Green's function method applicable to the modified Helmholtz operator.

3.1.2 Modified Helmholtz Equation

Suppose we have such a Helmholtz equation

$$\nabla^2 u - \lambda u = \phi(\mathbf{r}) \text{ in domain } \Omega, \tag{3.5}$$

with the boundary conditions on Γ

$$u = f_1(\mathbf{r}) \text{ on } \Gamma_1, \tag{3.6}$$

$$\frac{\partial u}{\partial n} = f_2(\mathbf{r}) \text{ on } \Gamma_2, \tag{3.7}$$

$$\gamma u + \frac{\partial u}{\partial n} = f_3(\mathbf{r}) \text{ on } \Gamma_3, \tag{3.8}$$

where $\Gamma_1 + \Gamma_2 + \Gamma_3 = \Gamma$.

Introducing the Green's function $G(\mathbf{r}, \mathbf{r}')$, the Green's function formation can be given as

$$\nabla^2 G - \lambda G = \delta(\mathbf{r}, \mathbf{r}') \text{ in domain } \Omega \tag{3.9}$$

with the boundary conditions

$$G = 0 \text{ on } \Gamma_1, \tag{3.10}$$

$$\frac{\partial G}{\partial n} = 0 \text{ on } \Gamma_2, \tag{3.11}$$

$$\gamma G + \frac{\partial G}{\partial n} = 0 \text{ on } \Gamma_3, \tag{3.12}$$

where $\delta(\mathbf{r}, \mathbf{r}')$ is *Dirac Delta function.*

Therefore, given the Green's function solutions defined in Eqs. 3.9 - 3.12, the modified Helmholtz equation 3.5 can be solved. After some mathematical derivation, we have

$$\begin{aligned} u(\mathbf{r}) = & \iint_\Omega G(\mathbf{r}, \mathbf{r}')\phi(\mathbf{r}')d\Omega' + \oint_{\Gamma_1} f_1(\mathbf{r}')\frac{\partial G(\mathbf{r}, \mathbf{r}')}{\partial n}d\Gamma' \\ & - \oint_{\Gamma_2} f_2(\mathbf{r}')G(\mathbf{r}, \mathbf{r}')d\Gamma' - \oint_{\Gamma_3} f_3(\mathbf{r}')G(\mathbf{r}, \mathbf{r}')d\Gamma' \end{aligned} \tag{3.13}$$

3.2 Green's Functions for Layered Reservoirs

3.2.1 Green's Function Formulation

In order to circumvent the complication of the formation configuration, we applied the Laplace transform and double Fourier cosine transform to obtain the Green's functions for the layered and composite systems.

We can rewrite Eq. 2.22 as

$$(\nabla_i^2 - \frac{s}{\kappa_i})\bar{p}_{Di} = 0, \tag{3.14}$$

where the Laplace operator ∇_i^2 is defined as

$$\nabla_i^2 = \frac{\partial^2}{\partial x_D^2} + (\lambda_y)_i \frac{\partial^2}{\partial y_D^2} + (\lambda_z)_i \frac{\partial^2}{\partial z_D^2}. \tag{3.15}$$

Using the Green's function formulation mentioned in Section 3.1, we can rewrite Eq. 3.14 (the subscript D is omitted for convenience) as

$$(\nabla_s^2 - \frac{s}{\kappa_s})\bar{G}_s(s, \mathbf{r}, \mathbf{r}') = -\delta(\mathbf{r} - \mathbf{r}'), \tag{3.16}$$

for the source layer (Layer i_s) and

$$(\nabla_i^2 - \frac{s}{\kappa_i})\bar{G}_i(s, \mathbf{r}, \mathbf{r}') = 0 \tag{3.17}$$

for the i-th layer ($i \neq i_s$).

The boundary and interface conditions become

$$\bar{G}_i(s, \mathbf{r}, \mathbf{r}') = 0 \text{ as x and y } \to \infty, \tag{3.18}$$

$$\bar{G}_i(s, \mathbf{r}, \mathbf{r}') = \bar{G}_{i+1}(s, \mathbf{r}, \mathbf{r}') \text{ at } z = z_i, \tag{3.19}$$

and

$$(\frac{k_z}{\mu})_i \frac{\partial \bar{G}_i}{\partial z}(s, \mathbf{r}, \mathbf{r}') = (\frac{k_z}{\mu})_{i+1} \frac{\partial \bar{G}_{i+1}}{\partial z}(s, \mathbf{r}, \mathbf{r}') \text{ at } z = z_i. \tag{3.20}$$

Eqs. 3.18, 3.19 and 3.20 apply for all layers, including the source layer.

For this type of problem, it is convenient to express the Green's function solution for the source layer as the sum of two solutions: 1) the solution to the partial differential equation with a point source (Eq. 3.16) and 2) the solution to the homogeneous equation (Eq. 3.17) for each layer. Thus the general solution for each layer is written as

$$\bar{G}_s(s, \mathbf{r}, \mathbf{r}') = \bar{G}_{ss}(s, \mathbf{r}, \mathbf{r}') + \bar{G}_{sh}(s, \mathbf{r}, \mathbf{r}'), \tag{3.21}$$

where $\bar{G}_{ss}$ is the point source response, $\bar{G}_{sh}$ is the homogeneous solution. The Green's function solution for no-source layers are solutions of homogeneous partial differential equation (Eq. 3.17) by themselves, so we can have

$$\bar{G}_i(s, \mathbf{r}, \mathbf{r}') = \bar{G}_{ih}(s, \mathbf{r}, \mathbf{r}'), \tag{3.22}$$

where $\bar{G}_{ih}$ is the homogeneous solution.

3.2.2 Solution of the Homogeneous Problem

The boundary condition given by Eq. 3.18 suggests the application of the double infinite Fourier cosine transform defined as

$$\bar{\bar{G}}_i(s,\alpha,\beta,z) = \int_0^\infty \int_0^\infty \bar{G}_i(s,x,y,z)\cos(\alpha x)\cos(\beta y)dxdy. \tag{3.23}$$

Applying the Fourier cosine transform to Eq. 3.17 for x and y yields

$$(\frac{\partial^2}{\partial z^2} - \nu_i^2)\bar{\bar{G}}_i(s,\alpha,\beta,z) = 0, \tag{3.24}$$

where

$$\nu_i^2 = \frac{1}{(\lambda_z)_i}[\alpha^2 + (\lambda_y)_i\beta^2 + \frac{s}{\kappa_i}]. \tag{3.25}$$

The boundary and interface conditions become

$$\bar{\bar{G}}_i(s,\alpha,\beta,z) = \bar{\bar{G}}_{i+1}(s,\alpha,\beta,z) \text{ at } z = z_i, \tag{3.26}$$

and

$$(\frac{k_z}{\mu})_i\frac{\partial\bar{\bar{G}}_i}{\partial z}(s,\alpha,\beta,z) = (\frac{k_z}{\mu})_{i+1}\frac{\partial\bar{\bar{G}}_{i+1}}{\partial z}(s,\alpha,\beta,z) \text{ at } z = z_i. \tag{3.27}$$

The solution of Eq. 3.24 can be written as

$$\bar{\bar{G}}_i(s,\alpha,\beta,z) = A_i\exp(\nu_i z) + B_i\exp(-\nu_i z), \tag{3.28}$$

where A_i and B_i will be determined from the boundary and interface conditions.

3.2.3 Point Source Solution

The point source response G_{ss} can be written as

$$G_{ss}(\mathbf{r},t;\mathbf{r}',t') = \frac{1}{4\sqrt{\pi[(t-t')/k_s]^3}} \exp[-\frac{k_s|\mathbf{r}-\mathbf{r}'|_s^2}{4(t-t')}], \tag{3.29}$$

where the normalized distance is defined as

$$|\mathbf{r}-\mathbf{r}'|_s^2 = (x-x')^2 + \frac{(y-y')^2}{(\lambda_y)_s} + \frac{(z-z')^2}{(\lambda_z)_s}. \tag{3.30}$$

The Laplace transform of the point source response, $\bar{G}_{ss}$, is

$$\bar{G}_{ss}(s,\mathbf{r};\mathbf{r}') = \frac{1}{|\mathbf{r}-\mathbf{r}'|_s} \exp[-\sqrt{s/\kappa_i}|\mathbf{r}-\mathbf{r}'|_s]. \tag{3.31}$$

The double Fourier transform of the point source reponse, $\bar{\bar{G}}_{ss}$, is

$$\bar{\bar{G}}_{ss}(s,\alpha,\beta,z;z') = \frac{\pi}{4\nu_s} \exp(-\nu_s|z-z'|). \tag{3.32}$$

3.2.4 Fundamental Point Source Solution

The point source solution for the source layer in a layered medium is obtained by substituting Eq. 3.28 and Eq. 3.32 in Eq. 3.21 as

$$\bar{\bar{G}}_s(s,\alpha,\beta,z;z') = \frac{\pi}{4\nu_s}[\exp(-\nu_s|z-z'|) + A_s\exp(\nu_s z) + B_s\exp(-\nu_s z)]. \tag{3.33}$$

The solution for the i-th layer ($i \neq i_s$) is given by Eq. 3.28.

The determination of A_i, B_i, A_s, and B_s coefficients is simple and they can be explicitly written out for a few layers. However, for more than a few layers, the computation task is more difficult. A new method, which is called *the reflection and transmission method*, is presented for determining the coefficients for n-layer systems in Section 3.3. Given the coefficients A_i, B_i, A_s and B_s, the general solution can be written for all layers, including the source layer (from Eq. 3.28 when $i \neq i_s$ and from Eq. 3.33 when $i = i_s$) as

$$\bar{G}_i(s,x,y,z;z') = \frac{4}{\pi^2}\int_0^\infty \int_0^\infty \bar{\bar{G}}_i(s,\alpha,\beta,z;z')\cos(\alpha(x-x'))\cos(\beta(y-y')).d\alpha d\beta \tag{3.34}$$

3.3 Reflection and Transmission Method

3.3.1 Local Transmission and Reflection Coefficients

In this section, we will employ a method commonly used to solve the wave equation in layered media, to obtain an alternate way of solving Eq. 3.24. This method has been presented by Kuchuck and Habashy [8] (see also Ref [19] for further detail). We did some further derivation on the homogeneous solutions in order to include the interaction between different layers in our solutions.

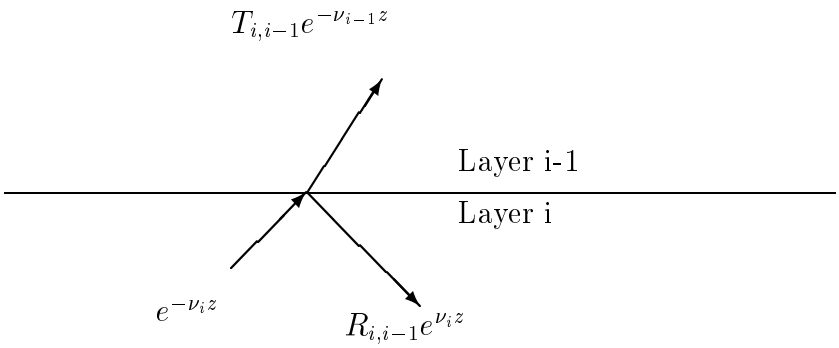

Figure 3.1: Local Transmission and Reflection

As shown in Fig. 3.3.1, at any interface boundary (discontinuity), the amplitude of the pressure field will change when it diffuses into another layer (transmission) and reflects back from the boundary (reflection). In Fig. 3.3.1 the incident wave (fundamental solution) $\exp(-\nu_i z)$ in the i-th layer is reflected as $R_{i,i-1}\exp(\nu_i z)$ and transmitted (diffused) as $T_{i,i-1}\exp(-\nu_{i-1}z)$ in a local coordinate system. The term R is the ratio of the amplitude of the reflected wave to the amplitude of the incident wave and the term T is the ratio of the amplitude of the transmitted wave to amplitude of the incident wave. As in the wave propagation, the incident, reflected, and transmitted waves should be understood as diffusion waves. For example, a point source in an infinite homogeneous medium propagates as an incident pressure diffusion wave without reflection and transmission.

For each layer, there will a local coordinate system, in which the origin of the z coordinate is assumed to be at the interface of the two adjacent layers. Substituting these solutions in Eq. 3.26 (the pressure interface condition) yields

$$1 + R_{i,i-1} = T_{i,i-1}, \tag{3.35}$$

which states that the incident pressure diffusion wave plus the reflected wave is equal to what is transmitted to the adjacent layer i-1. Similarly, using the flux interface condition given by Eq. 3.27, we obtain

$$(\frac{k_z}{\mu})_i(-\nu_i + \nu_i R_{i,i-1}) = -(\frac{k_z}{\mu})_{i-1}\nu_{i-1}T_{i,i-1}. \tag{3.36}$$

The solution of Eqs. 3.26 and 3.27 gives the local reflection and transmission coefficients as

$$R_{i,i-1} = \frac{\nu_i - \gamma_{i-1,i}\nu_{i-1}}{\nu_i + \gamma_{i-1,i}\nu_{i-1}}, \tag{3.37}$$

$$R_{i,i-1} = \frac{2\nu_i}{\nu_i + \gamma_{i-1,i}\nu_{i-1}}, \tag{3.38}$$

where

$$\gamma_{i-1,i} = \frac{(k_z/\mu)_{i-1}}{(k_z/\mu)_i}, \tag{3.39}$$

and $R_{i,i-1} = 1$ if the $(i-1)$-th is a no-flow boundary since the incident wave is totally reflected, and $R_{i,i-1} = -1$ if the the $(i-1)$-th layer is constant-pressure boundary. The terms $R_{i,i-1}$ and $T_{i,i-1}$ are referred to as the *local reflection and transmission coefficients*, respectively.

3.3.2 The Green's Function for the Source Layer

The solution for the source layer is given by Eq. 3.33 as

$$\bar{\bar{G}}_s(z; z_s) = \frac{\pi}{4\nu_s}[\exp(-\nu_s|\hat{z}|) + A_s \exp(\nu_s\hat{z}) + B_s \exp(-\nu_s\hat{z})], \tag{3.40}$$

where $\hat{z} = z - z_s$ (z_s is the offset of the point source), and $\bar{\bar{G}}_s(z, z_s)$ is a shorthand notation for $\bar{\bar{G}}_s(s, \alpha, \beta, z, z_s)$. For $0 < z < z_s$ ($\hat{z} < 0$), Eq. 3.40 becomes

$$\bar{\bar{G}}_s(z; z_s) = \frac{\pi}{4\nu_s}[\exp(\nu_s \hat{z}) + A_s \exp(\nu_s \hat{z}) + B_s \exp(-\nu_s \hat{z})]. \tag{3.41}$$

From this equation, a downgoing global reflection coefficient (see Fig. 3.3.2) at the boundary is defined as

$$(R_D)_s = \frac{B_s \exp(-\nu_s \hat{z})}{\exp(\nu_s \hat{z}) + A_s \exp(\nu_s \hat{z})} \mid_{z=0} . \tag{3.42}$$

Eq. 3.42 can be further simplified as

$$(R_D)_s = \frac{B_s}{1 + A_s} \exp(2\nu_s z_s). \tag{3.43}$$

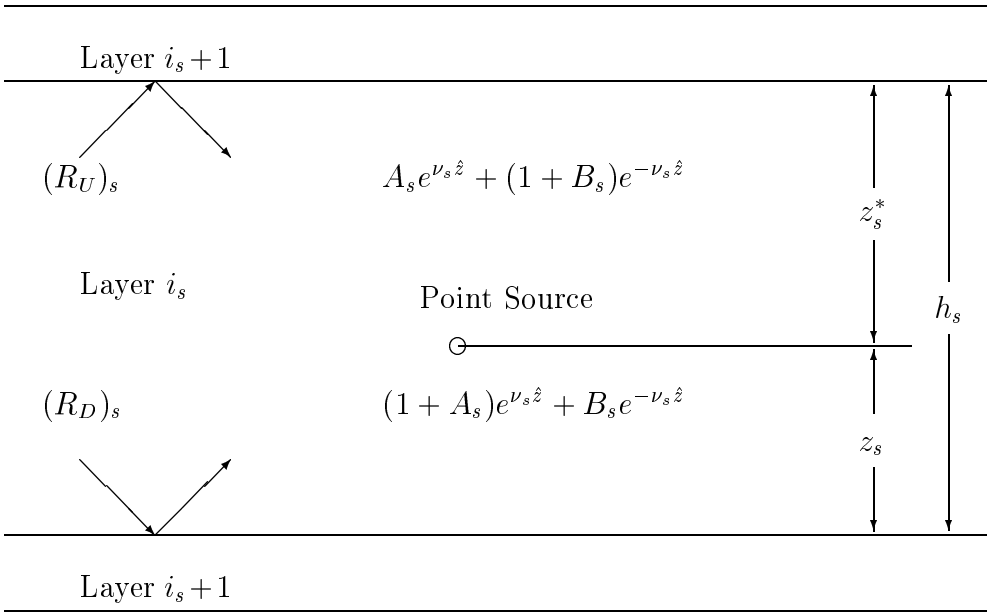

Figure 3.2: Global Reflection Coefficients in Source Layer

Similarly for $z_s < z < h_s$, an upgoing global reflection coefficient (see Fig. 3.3.2) at the boundary can also be defined from Eq. 3.40 as

$$(R_U)_s = \frac{A_s}{1 + B_s} \exp(2\nu_s z_s^*), \tag{3.44}$$

where $z_s^* = h_s - z_s$, D and U denote downgoing and upgoing pressure diffusion waves, respectively.

Solving Eqs. 3.43 and 3.44 for A_s and B_s yields

$$A_s = \frac{1 + (R_D)_s \exp(-2\nu_s z_s)}{1 - (R_U)_s (R_D)_s \exp(-2\nu_s h_s)} (R_U)_s \exp(-2\nu_s z_s^*), \tag{3.45}$$

$$B_s = \frac{1 + (R_U)_s \exp(-2\nu_s z_s^*)}{1 - (R_U)_s (R_D)_s \exp(-2\nu_s h_s)} (R_D)_s \exp(-2\nu_s z_s). \tag{3.46}$$

Given the coefficients A_s and B_s, the homogeneous solution for the source layer from Eq. 3.40 can be written as

$$\begin{aligned} \bar{\bar{G}}_{sh}(z; z') = & \frac{\pi}{4\nu_s} \frac{1}{1 - (R_U)_s (R_D)_s \exp(-2\nu_s h_s)} \\ & \{[1 + (R_D)_s \exp(-2\nu_s z_s)](R_U)_s \exp(-\nu_s z_s^*) \exp(-\nu_s z^*) \\ & + [1 + (R_U)_s \exp(-2\nu_s z_s^*)](R_D)_s \exp(-\nu_s z_s) \exp(-\nu_s z)\}, \end{aligned} \tag{3.47}$$

where $z^* = h_s - z$, $(R_D)_s$ and $(R_U)_s$ are global reflection coefficients to be determined later. The coefficients for other layers are obtained in next section.

3.3.3 Determination of Coefficients

In the local coordinate system (see Fig. 3.3.4), the solution for the i-th layer ($0 < z_i < h_i$) from Eq. 3.28 can be written as

$$\bar{\bar{G}}_i(z) = A_i \exp(\nu_i z_i) + B_i \exp(-\nu_i z_i). \tag{3.48}$$

From this equation, the upgoing global reflection coefficient for the i-th layer can defined as

$$(R_U)_i = \frac{A_i \exp(\nu_i z_i)}{B_i \exp(-\nu_i z_i)} \,|_{z_i = h_i} = \frac{A_i}{B_i} \exp(2\nu_i h_i). \tag{3.49}$$

Solving Eq. 3.49 for A_i and substituting the result in Eq. 3.48 gives

$$\bar{\bar{G}}_i(z) = B_i \{\exp(-\nu_i z_i) + (R_U)_i \exp[-\nu_i (2h_i - z_i)]\}, \tag{3.50}$$

and similarly for the $i-1$th layer ($0 < z_{i-1} < h_{i-1}$)

$$\bar{\bar{G}}_{i-1}(z) = B_{i-1}\{\exp(-\nu_{i-1}z_{i-1}) + (R_U)_{i-1}\exp[-\nu_{i-1}(2h_{i-1} - z_{i-1})]\}. \tag{3.51}$$

From the interface condition Eq. 3.26, we can have

$$\bar{\bar{G}}_i(h_i) = \bar{\bar{G}}_{i-1}(0), \tag{3.52}$$

thus we obtain a recurrence relation for B_i as

$$\frac{B_{i-1}}{B_i} = \frac{1 + (R_U)_i}{1 + (R_U)_{i-1}\exp(-2\nu_{i-1}h_{i-1})}\exp(-\nu_i h_i). \tag{3.53}$$

For the source layer, the definition of B is different from B_s in Eq. 3.46. For $z_s < z < h_s$, Eq. 3.40 becomes

$$\bar{\bar{G}}_s(z; z_s) = \frac{\pi}{4\nu_s}\{(1 + B_s)\exp[-\nu_s(z - z_s)] + A_s\exp[\nu_s(z - z_s)]\}. \tag{3.54}$$

Substituting Eq. 3.44, we have

$$\bar{\bar{G}}_s(z; z_s) = \frac{\pi}{4\nu_s}(1 + B_s)\exp(\nu_s z_s)\{\exp(-\nu_s z) + (R_U)_s\exp[-\nu_s(2h_s - z)]\}. \tag{3.55}$$

Thus the equivalent upgoing reflection coefficient for the source layer, B_s^* is defined as

$$B_s^* = \frac{\pi}{4\nu_s}(1 + B_s)\exp(\nu_s z_s), \tag{3.56}$$

or

$$B_s^* = \frac{\pi}{4\nu_s}\frac{1 + (R_D)_s\exp(-2\nu_s z_s)}{1 - (R_U)_s(R_D)_s\exp(-2\nu_s h_s)}\exp(\nu_s z_s). \tag{3.57}$$

Using the recurrence relation given in Eq. 3.53, we can obtain the coefficient B_i for the layers above the source layer ($i < i_s$). So

$$\bar{\bar{G}}_i(z) = B_i\{\exp(-\nu_i z_i) + (R_U)_i\exp[-\nu_i(2h_i - z_i)]\} \tag{3.58}$$

Similarly, we can obtain another recurrence relation for A_i as

$$\frac{A_i}{A_{i-1}} = \frac{1 + (R_D)_{i-1}}{1 + (R_D)_i\exp(-2\nu_i h_i)}\exp(-\nu_i h_i). \tag{3.59}$$

For $0 < z < z_s$, Eq. 3.40 becomes

$$\bar{\bar{G}}_s(z; z_s) = \frac{\pi}{4\nu_s}\{(1 + A_s)\exp[\nu_s(z - z_s)] + B_s \exp[-\nu_s(z - z_s)]\}. \tag{3.60}$$

Substituting Eq. 3.43 , we have

$$\bar{\bar{G}}_s(z; z_s) = \frac{\pi}{4\nu_s}(1 + A_s)\exp(-\nu_s z_s)[\exp(\nu_s z) + (R_D)_s \exp(-\nu_s z)], \tag{3.61}$$

so

$$A_s^* = \frac{\pi}{4\nu_s}(1 + A_s)\exp(-\nu_s z_s), \tag{3.62}$$

or

$$A_s^* = \frac{\pi}{4\nu_s}\frac{1 + (R_U)_s \exp(-2\nu_s z_s^*)}{1 - (R_U)_s(R_D)_s \exp(-2\nu_s h_s)}\exp(-\nu_s z_s). \tag{3.63}$$

Therefore we obtained a similar equation as

$$\bar{\bar{G}}_i(z) = A_i[\exp(\nu_i z_i) + (R_D)_i \exp(-\nu_i z_i)]. \tag{3.64}$$

3.3.4 Calculation of Global Reflection Coefficients

In order to evaluate the solutions given by Eqs. 3.47, 3.58, and 3.64, the upgoing and downgoing global reflection coefficients must be determined. Using the solutions given by Eqs. 3.50 and 3.51, the relationships at interface (see Fig. 3.3.4) can be written. For the (i-1)-th layer,

$$T_{i,i-1}B_i \exp(-\nu_i h_i) + R_{i-1,i}B_{i-1}(R_U)_{i-1}\exp(-2\nu_{i-1}h_{i-1}) = B_{i-1}. \tag{3.65}$$

This equation is evaluated at $z_{i-1} = 0$ (z is in the local coordinates). For the i-th layer,

$$R_{i,i-1}B\exp(-\nu_i h_i) + T_{i-1,i}B_{i-1}(R_U)_{i-1}\exp(-2\nu_{i-1}h_{i-1}) = B_i(R_U)_i \exp(-\nu_i h_i). \tag{3.66}$$

Solving the two equations above for $(R_U)_i$, we obtain

$$(R_U)_i = R_{i,i-1} + \frac{T_{i,i-1}\exp(-\nu_{i-1}h_{i-1})(R_U)_{i-1}\exp(-\nu_{i-1}h_{i-1})T_{i-1,i}}{1 - R_{i-1,i}(R_U)_{i-1}\exp(-2\nu_{i-1}h_{i-1})}. \tag{3.67}$$

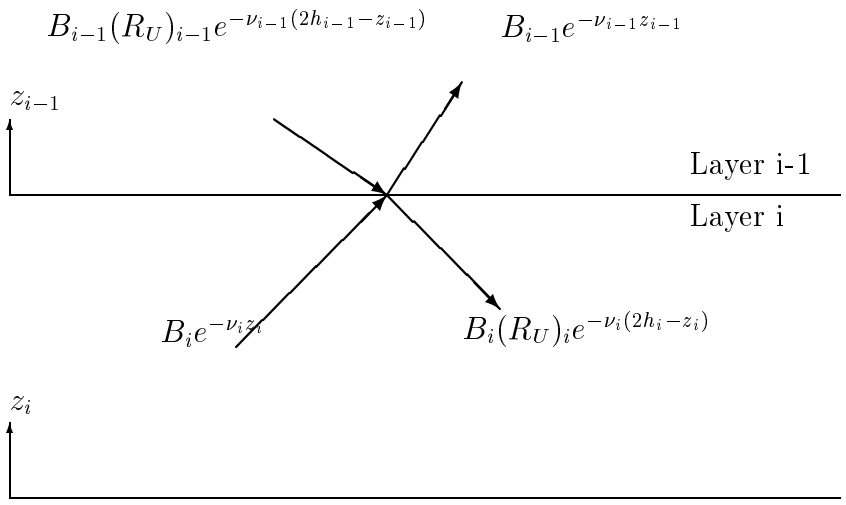

Figure 3.3: Reflected and Transmitted Solutions in a Local Coordinate System

Substituting Eq. 3.35 in Eq. 3.67 and $R_{i,i-1}$ for $-R_{i-1.i}$, gives

$$(R_U)_i = \frac{R_{i,i-1} + (R_U)_{i-1}\exp(-2\nu_{i-1}h_{i-1})}{1 + R_{i,i-1}(R_U)_{i-1}\exp(-2\nu_{i-1}h_{i-1})}, \tag{3.68}$$

where i = 2,3,...,n.

At the top boundary, we can obtain $(R_U)_1$ as

$$(R_U)_1 = 1 \text{ at the no-flow boundary} \tag{3.69}$$

and

$$(R_U)_1 = -1 \text{ at the constant-pressure boundary} \tag{3.70}$$

For the downgoing reflection coefficient $(R_D)_i$, we have a similar recurrence relation as

$$(R_D)_i = \frac{1/R_{i,i+1} + (R_D)_{i+1}\exp(-2\nu_{i+1}h_{i+1})}{1 + 1/R_{i,i+1}(R_D)_{i+1}\exp(-2\nu_{i+1}h_{i+1})}, \tag{3.71}$$

where i = 1,2,...,n-1.

At the bottom boundary, we can obtain $(R_D)_n$ as

$$(R_D)_n = 1 \text{ at the no-flow boundary,} \tag{3.72}$$

and

$$(R_D)_n = -1 \text{ at the constant-pressure boundary.} \tag{3.73}$$

It is also possible to have an infinitely thick layer (in the z direction) either at the top of the first layer, beneath the bottom layer, or both. For this case, the global reflection coefficient for the top layer (the infinitely thick layer is at the top) becomes

$$(R_U)_1 = \frac{\nu_1 - \gamma_{0,1}\nu_0}{\nu_1 + \gamma_{0,1}\nu_0}, \tag{3.74}$$

or the global reflection coefficient for the bottom layer (the infinitely thick layer is at the bottom) becomes

$$(R_D)_n = \frac{\nu_n - \gamma_{n+1,n}\nu_{n+1}}{\nu_n + \gamma_{n+1,n}\nu_{n+1}}, \tag{3.75}$$

where 0 and $n+1$ denote the top and bottom infinite layer properties respectively.

Section 4

Slanted Wells in Multilayered Reservoirs

4.1 Problem Description

This study concerns the pressure-transient behaviors of a slanted well in a multilayered reservoir with crossflow, while the well may or may not cross interfaces between layers. Since crossflow is permitted on the interfaces, there is communication between these layers. Therefore we have to consider the interaction between the well segments in different layers, which can not be solved using conventional methods.

Let us consider a layered reservoir consisting of several infinite anisotropic horizontal layers. The reservoir is bounded by no-flow or constant-pressure boundaries. A slanted well crossing several layers is completed in this reservoir, and the center of the well is the origin of the global coordinate system. The inclination angle of the well (deviated from the horizontal direction) is θ_w. The configuration of the reservoir is shown in Fig. 4.1.

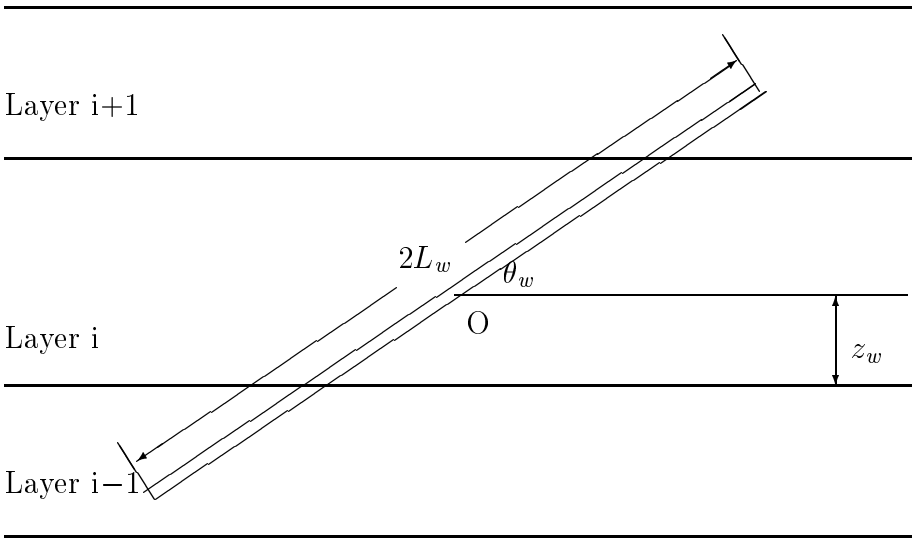

Figure 4.1: Configuration of a Slanted Well

4.2 Segmentation Technique

In our study, we used the infinite-conductivity boundary condition on the wellbore, so the segmentation method was used to discretize the wellbore into several segments and each segment was treated as having uniform flux (see Fig. 4.2). The pressure drop along the wellbore is uniform to satisfy the infinite-conductivity inner boundary. Based on this assumption, we can derive the discretization equations for pressure drop of each segment in the Laplace space.

The pressure drop at the midpoint of each segment is assumed the same along the wellbore, so the infinite-conductivity constraint along the wellbore yields

$$\Delta p_i(t) = \Delta p(t), \tag{4.1}$$

where $i = 1, ..., m$, and m is the number of the segments in the well. We denote $\Delta p_i(t)$

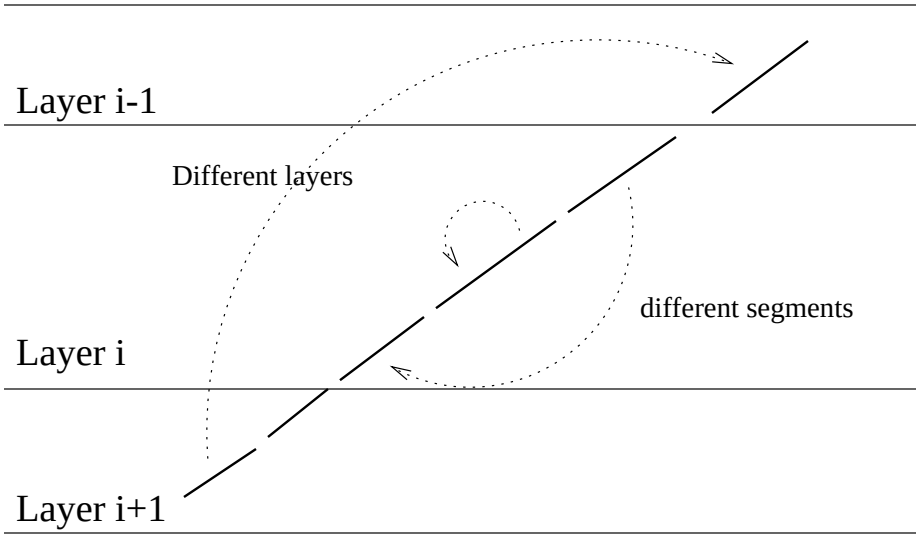

Figure 4.2: Segmentation for a Slanted Well

as the pressure drop at the midpoint of Segment i and $\Delta p(t)$ as the total pressure drop of the well (downhole pressure drop).

Based on the material balance in the wellbore, the summation of the flux along each segment should be equal to the total flow rate of the well, so the flow rate constraint is given as

$$\sum_{i=1}^{m} l_i \cdot q_i(t) = Q, \tag{4.2}$$

where l_i is the length of Segment i, and $q_i(t)$ is the flux along Segment i, and Q is the total flow rate (a constant for flow-control production).

Applying the Laplace transform to Eqs. 4.1 and 4.2 yields

$$\Delta\bar{p}_i(s) = \Delta\bar{p}(s), \tag{4.3}$$

and

$$\sum_{i=1}^{m} l_i \cdot \bar{q}_i(s) = Q/s, \tag{4.4}$$

The pressure drop along the wellbore is the superposition of the effects of all the segments of the wellbore, so it is a linear combination of the convolution product of the flux and the perturbation (in this case, the Green's function), thus we have

$$\Delta p_i(t) = \sum_{j=1}^{m} G_{ij}(t) * q_j(t), \tag{4.5}$$

where G_{ij} is defined as the perturbation on the midpoint of Segment i induced by Segment j, and the symbol $"*"$ denotes the convolution product of two functions, defined as

$$f(t) * g(t) = \int_0^t f(\tau) \cdot g(t-\tau) d\tau. \tag{4.6}$$

and the convolution product has a deconvolution property for the Laplace transform defined as

$$\mathcal{L}[f(t) * g(t)] = \mathcal{L}[f(t)] \cdot \mathcal{L}[g(t)], \tag{4.7}$$

so in the Laplace space, the convolution relation between input and output can be deconvolved as

$$\Delta \bar{p}_i(s) = \sum_{j=1}^{m} \bar{G}_{ij}(s) \cdot \bar{q}_j(s). \tag{4.8}$$

Combining Eqs. 4.3, 4.4 and 4.8, we have a linear equation for $\bar{p}(s)$ and $\bar{q}_i(s)$ as

$$\begin{bmatrix} G_{n\times n} & -\mathbf{J}_n \\ \mathbf{L}_n^T & 0 \end{bmatrix} \cdot \begin{bmatrix} \bar{\mathbf{q}}_n \\ \Delta\bar{p} \end{bmatrix} = \begin{bmatrix} \mathbf{0}_n \\ Q/s \end{bmatrix}, \tag{4.9}$$

where $G_{n\times n}$ is the matrix of the Green's functions defined as

$$G_{n\times n} = \begin{bmatrix} \bar{G}_{11} & \bar{G}_{12} & \cdots & \bar{G}_{1n} \\ \vdots & \vdots & \ddots & \vdots \\ \bar{G}_{n1} & \bar{G}_{n2} & \cdots & \bar{G}_{nn} \end{bmatrix}, \tag{4.10}$$

and $\mathbf{J}_n = [1, 1, \ldots, 1]^T$, $\mathbf{L}_n = [l_1, l_2, \ldots, l_n]^T$.

Rearraying and solving Eq. 4.9 yields

$$\Delta\bar{p} = (\mathbf{L}^T G^{-1} \mathbf{J})^{-1} \cdot Q/s, \tag{4.11}$$

$$\bar{\mathbf{q}} = G^{-1}\mathbf{J} \cdot \Delta\bar{p}. \tag{4.12}$$

In practice, we did not calculate the inversion of G, which is time-consuming, instead we solved a linear equation

$$G \cdot \mathbf{U} = \mathbf{J}, \tag{4.13}$$

to obtain $\mathbf{U}$, where $\mathbf{U} = G^{-1} \cdot \mathbf{J}$. Thus the solutions for Eq. 4.9 become

$$\Delta\bar{p} = (\mathbf{L}^T\mathbf{U})^{-1} \cdot Q/s, \tag{4.14}$$

$$\bar{\mathbf{q}} = \mathbf{U} \cdot \Delta\bar{p}. \tag{4.15}$$

Therefore, given all the Green's functions, we can obtain the pressure drop $\bar{p}(s)$ for an arbitrary Laplace variable. After obtaining a set of pressure drop data in the Laplace space, we can process the inverse Laplace transform to obtain the pressure drop solution. The Stehfest algorithm [23][24] is a very good choice for such a problem. The calculation of the Green's functions is described in next section.

4.3 Green's Function for Segments

In order to process the calculation of the pressure drop in the Laplace space presented in previous section, we need to calculate the Green's functions induced by a segment (a line source), instead of a single point source. Unfortunately, we do not have the Green's functions for the solutions to the homogeneous equations in the Laplace space, so we have to deal with them separately.

From Eq. 3.21, we can have the Green's function $\bar{G}(s, \mathbf{r}, \mathbf{r}')$ (perturbation on point $\mathbf{r}'$ induced by point source located at $\mathbf{r}$) as

$$\bar{G}(s, \mathbf{r}, \mathbf{r}') = \bar{G}_{ss}(s, \mathbf{r}, \mathbf{r}') + \bar{G}_{sh}(s, \mathbf{r}, \mathbf{r}'), \tag{4.16}$$

for the point source and the affected point are in the same layer, otherwise

$$\bar{G}(s, \mathbf{r}, \mathbf{r}') = \bar{G}_{ih}(s, \mathbf{r}, \mathbf{r}'). \tag{4.17}$$

The Green's function $\bar{G}_{ij}$ is the perturbation on the midpoint of Segment j induced by Segment i, so we have the relation as

$$\bar{G}_{ij} = \int_{L_i} \bar{G}(s, \mathbf{r}, \mathbf{r_j}) dl = < G(s, \mathbf{r}, \mathbf{r_j}) >_i, \tag{4.18}$$

where $\mathbf{r_j}$ is the midpoint of Segment j.

For the homogeneous solutions, we have

$$\bar{G}_h(s, \mathbf{r}, \mathbf{r}') = \frac{4}{\pi^2} \int_0^\infty \int_0^\infty \bar{\bar{\bar{G}}}_h(s, \alpha, \beta, z; z') \cos(\alpha(x - x')) \cdot d\alpha d\beta \tag{4.19}$$

so we have

$$\begin{aligned} < \bar{G}_h(s, \mathbf{r}, \mathbf{r_j}) >_i &= \int_{L_i} dl \cdot \{ \frac{4}{\pi^2} \int_0^\infty \int_0^\infty d\alpha d\beta \cdot \bar{\bar{\bar{G}}}_h(s, \alpha, \beta, z; z_j) \cos(\alpha(x - x_j)) \} \\ &= \frac{4}{\pi^2} \int_0^\infty \int_0^\infty d\alpha d\beta \cdot \int_{L_i} dl \cdot \bar{\bar{\bar{G}}}_h(s, \alpha, \beta, z; z_j) \cos(\alpha(x - x_j)) \\ &= \frac{4}{\pi^2} \int_0^\infty \int_0^\infty d\alpha d\beta \cdot S(s, \alpha, \beta), \end{aligned} \tag{4.20}$$

where

$$S(s, \alpha, \beta) = \int_{L_i} dl \cdot \bar{\bar{\bar{G}}}_h(s, \alpha, \beta, z; z_j) \cos(\alpha(x - x_j)), \tag{4.21}$$

and

$$x = x_i + l \cdot \cos\theta_w, \tag{4.22}$$

$$z = z_i + l \cdot \sin\theta_w. \tag{4.23}$$

Eq. 4.21 can be integrated analytically and expressed in a form as

$$S(s, \alpha, \beta) = Cterm \cdot (Aterm + Bterm), \tag{4.24}$$

where *Aterm, Bterm* and *Cterm* are functions of α and β (other variables are constants regarding the integral), and are given in the next part.

4.3.1 Green's Function for Segments in Same Layer

If two segments, Segment i and Segment j are in the same layer, Eq. 4.18 becomes

$$\bar{G}_{ij} =< \bar{G}_{ss}(s, \mathbf{r}, \mathbf{r_j}) >_i + < \bar{G}_{sh}(s, \mathbf{r}, \mathbf{r_j}) >_i . \tag{4.25}$$

Eq. 3.47 is rewritten as

$$\begin{aligned} \bar{\bar{G}}_{sh}(z_j; z) &= \frac{\pi}{4\nu_s} \frac{1}{1 - (R_U)_s (R_D)_s \exp(-2\nu_s h_s)} \\ &\cdot \{[\exp(\nu_s z_j) + (R_D)_s \exp(-\nu_s z_j)](R_U)_s \exp(-2\nu_s h_s) \exp(\nu_s z) \\ &+ [\exp(-\nu_s z_j) + (R_U)_s \exp(-\nu_s(2h_s - z_j))](R_D)_s \exp(-\nu_s z)\}. \end{aligned} \tag{4.26}$$

After some mathematical derivation, we have

$$Cterm = \frac{\pi}{4\nu_s} \frac{1}{1 - (R_U)_s (R_D)_s \exp(-2\nu_s h_s)}, \tag{4.27}$$

$$Aterm = Jterm_+ \cdot [\exp(-\nu_s(h_s - z_j)) + (R_D)_s \exp(-\nu_s(h_s + z_j))] \cdot (R_U)_s \exp(-\nu_s h_s), \tag{4.28}$$

and

$$Bterm = Jterm_- \cdot [\exp(-\nu_s z_j) + (R_U)_s \exp(-\nu_s(2h_s - z_j))] \cdot (R_D)_s, \tag{4.29}$$

where $Jterm_\pm$ is an integral defined as

$$\begin{aligned} Jterm_\pm &= \int_{L_i} \exp(\pm\nu_s z) \cos(\alpha(x - x_j)) dl \\ &= \int_{-l_i/2}^{l_i/2} \exp(\pm\nu_s(z_i + l \sin\theta_w)) \cos(\alpha(x_i - x_j + l\cos\theta_w)) dl \\ &= \frac{\exp(\pm(\nu_s z_i + a \cdot l))}{a^2 + b^2} [\pm a \cos(b \cdot l + c) + b \sin(b \cdot l + c)] \,|_{-l_i/2}^{l_i/2} . \end{aligned} \tag{4.30}$$

In Eq. 4.30, variables a, b and c are defined as

$$a = \nu_s \sin\theta_w, \tag{4.31}$$

$$b = \alpha \cos\theta_w, \tag{4.32}$$

$$c = \alpha(x_i - x_j). \tag{4.33}$$

4.3.2 Green's Function for Segments in Different Layers

If Segment i and Segment j are in different layers, then Eq. 4.18 becomes

$$\bar{G}_{ij} =< \bar{G}_{jh}(s, \mathbf{r}, \mathbf{r_j}) >_i . \tag{4.34}$$

The solutions are different for $i < j$ and $i > j$.

At first, for $j < i$, from Eqs. 3.50, 3.57, we have

$$Cterm = \frac{\pi}{4\nu_s} \frac{\exp(-\nu_j z_j) + (R_U)_j \exp[-\nu_j(2h_j - z_j)]}{1 - (R_U)_s (R_D)_s \exp(-2\nu_s h_s)} \prod_{k=Nj+1}^{Ni} \frac{B_{k-1}}{B_k} \tag{4.35}$$

$$Aterm = Jterm_+, \tag{4.36}$$

and

$$Bterm = Jterm_- \cdot (R_D)_s. \tag{4.37}$$

where N_i denotes the layer in which Segment i is located, and B_{k-1}/B_k is given by Eq. 3.53.

Secondly, for $j > i$, from Eqs. 3.50, 3.57, we have

$$Cterm = \frac{\pi}{4\nu_s} \frac{\exp(\nu_j z_j) + (R_D)_j \exp[-\nu_j z_j]}{1 - (R_U)_s (R_D)_s \exp(-2\nu_s h_s)} \prod_{k=N_i+1}^{N_j} \frac{A_k}{A_{k-1}} \tag{4.38}$$

$$Aterm = Jterm_+ \cdot (R_U)_s \exp(-2\nu_s h_s), \tag{4.39}$$

and

$$Bterm = Jterm_-. \tag{4.40}$$

where A_k/A_{k-1} is given by Eq. 3.59.

4.3.3 Solutions for Single-Layered Reservoirs

The situation will be simplified very much if the reservoir is single-layered and bounded by constant-pressure or no-flow boundaries. In this case, the Green's solutions can be given easily in the real space. The detail has been presented by Gommard [17], it

is presented here briefly for completeness (no results and discussion of this method are given here).

The point source solution of a single-layered transversely isotropic reservoir can be given as the product of a infinite line source solution (taken in the vertical solution) and a plane source solution in a slab reservoir (the plane is horizontal). Suppose the point source is located at point $P(x', y', z')$ and the affected point is located at point $M(x, y, z)$. The point source is given as

$$S(\mathbf{r}, \mathbf{r}', t) = SP(z, z', t) \cdot I(\rho, t). \tag{4.41}$$

In Eq. 4.41, the line source solution $I(\rho, t)$ is given as

$$I(\rho, t) = \frac{\exp(-\frac{\rho^2}{4\eta_h t})}{4\pi\eta_h t}, \tag{4.42}$$

where

$$\rho^2 = (x - x')^2 + (y - y')^2, \tag{4.43}$$

and the plane source solution is given as

$$SP(z, z', t) = \begin{cases} SP_1(z, z', t) & \text{for small t;} \\ SP_2(z, z', t) & \text{for large t} \end{cases}, \tag{4.44}$$

where

$$SP_1(z, z', t) = \frac{1}{\sqrt{4\pi\eta_z t}} \sum_{n=-\infty}^{+\infty} [\exp(-\frac{(z - z' + 2nh)^2}{4\eta_z t}) + \exp(-\frac{(z + z' + 2nh)^2}{4\eta_z t})], \tag{4.45}$$

$$SP_2(z, z', t) = \frac{1}{h}[1 + 2 \sum_{n=-\infty}^{+\infty} \exp(-\frac{(n\pi)^2 \eta_z t}{h^2} \cos\frac{n\pi z}{h} \cos\frac{n\pi z'}{h})]. \tag{4.46}$$

Both the infinite series shown in Eqs. 4.45 and 4.46 can converge very quickly, but this property can not be preserved in the Laplace space. The strategy is to process the Laplace transform on the point source solution using a numerical algorithm instead of obtaining analytical transform solutions for each term.

Given the Green's functions in the Laplace space, we can use the segmentation technique presented in Section 4.2 to solve the problem.

4.3.4 Well Pressure Response

Slanted wells may have a considerable wellbore volume below the tool even when a shut-in device is used or the downhole flow rate is measured. Thus the wellbore pressure is given by

$$p_{wD}(t_D) = \int_0^{t_D} [q_{mD}(\tau) - C_{DL}\frac{dp_{wD}(\tau)}{d\tau}]p'_{SD}(t_D - \tau)d\tau, \tag{4.47}$$

and its Laplace transform is

$$\bar{p}_{wD}(s) = s \cdot \bar{q}_{mD}(s)\frac{\bar{p}_{SD}(s)}{1 + C_{DL}s^2\bar{p}_{SD}(s)}, \tag{4.48}$$

where $q_{mD}(s)$ is the measured normalized flow rate (q_m/q_r) and

$$p_{SD}(t_D) = p_D(t_D) + S, \tag{4.49}$$

and S is the skin factor of the wellbore.

Eq. 4.49 yields

$$p'_{SD}(t_D) = p'_D(t_D) + S\delta(t_D), \tag{4.50}$$

where $\delta(t_D)$ is the Dirac delta function and p_D is the constant-rate dimensionless sandface pressure (given by Eq. 4.9).

The dimensionless storage coefficient C_{DL} is given by

$$C_{DL} = \frac{5.615C}{4\pi(\phi c_t)_r L_w^3}, \tag{4.51}$$

where the storage coefficient C is defined using the wellbore volume below the measuring point. If q_{mD} measured at the wellhead is constant, Eq. 4.47 becomes the well-known wellbore pressure solution with storage and skin [21],[22] as

$$p_{wD}(t_D) = \int_0^{t_D} [1 - C_{DL}\frac{dp_{wD}(\tau)}{d\tau}]p'_{SD}(t_D - \tau)d\tau, \tag{4.52}$$

and its Laplace transform is

$$\bar{p}_{wD}(s) = \frac{\bar{p}_{SD}(s)}{1 + C_{DL}s^2\bar{p}_{SD}(s)}, \tag{4.53}$$

where C_{DL} is defined using the total wellbore volume.

The wellbore pressure given by Eq. 4.47 or its Laplace transform are used for the interpretation of downhole pressure and flow rate measurements. Eq. 4.52 and its Laplace transform are used if the downhole flow rate is not available.

The definition of the skin factor in Eq. 4.49 becomes more complicated for slanted wells in multilayered reservoirs, due to the different properties of the layers. The damage to wellbores varies in different layers, so an effective skin factor may be necessary in this case. Furthermore, the skin factor may be also a function of time, due to different flow distributions along the wellbore at different flow regimes. Such situations are still under investigation.

4.4 Results and Discussion

The behaviors of several multilayered systems were evaluated using the solution presented above. For all examples, the wellbore length $2L_w$ is 1000 ft and radius r_w is 0.35 ft. The formation and fluid properties for these examples are given in Table 4.4.

4.4.1 Impact of Subdivision of Segments

In Section 4.2, we presented the segmentation technique, which depends on the subdivision of segments, so different subdivision schemes may lead to different results. Therefore we studied the impact of different subdivisions on the performance and obtained an optimal choice of segments.

Through our study, the wellbore in each layer (the wellbore may cross several layers, we have to treat them respectively) was divided into $2n$ segments of variable lengths. The length distribution was based on a geometric suite with a ratio of X_{ratio}, which is defined as

$$l_1 = l_{2n}, \tag{4.54}$$

$$l_{i+1} = l_{2n-i} = X_{ratio} l_i \text{ for } 1 \leq i \leq n-1, \tag{4.55}$$

No.	Layer	$h(ft)$	$k_h(md)$	$k_v(md)$
1	1	100	100	1
2	1(r)	100	100	1
	2	100	200	10
3(a)	1	50	100	1
	2(r)	50	200	10
	3	50	100	1
3(b)	1	40	100	1
	2(r)	70	200	10
	3	40	100	1
4	1	40	160	20
	2	20	100	16
	3	10	60	12
	4(r)	20	100	10
	5	30	40	4
	6	10	20	2

Table 4.1: Reservoir Parameters for Slanted Wells

$$\sum_{i=1}^{2n} l_i \quad = \quad l_w, \tag{4.56}$$

where l_i denotes the length of each segment and l_w is the length of the wellbore in that layer.

Roemershauser [12] showed that the surface flow is higher at the ends of the well than in the middle, due to the larger flow area around the ends. Furthermore, in layered reservoirs, the interaction at the interfaces is an important factor on the performance. Therefore, it is reasonable to choose a distribution factor $X_{ratio} > 1$ (typically, $X_{ratio} = 2$).

Let us consider a slanted well ($\theta_w = 5^o$) with a 50-ft standoff located a single-layered reservoir with no-flow boundaries at the top and the bottom, and the formation properties as defined in Table 4.4 ($No.$ 1). We investigated the pressure derivatives using different segmentation schemes, and compared the behavior of a fine subdivision (32 segments) with a coarse subdivision (8 segments, $X_{ratio} = 1$ or

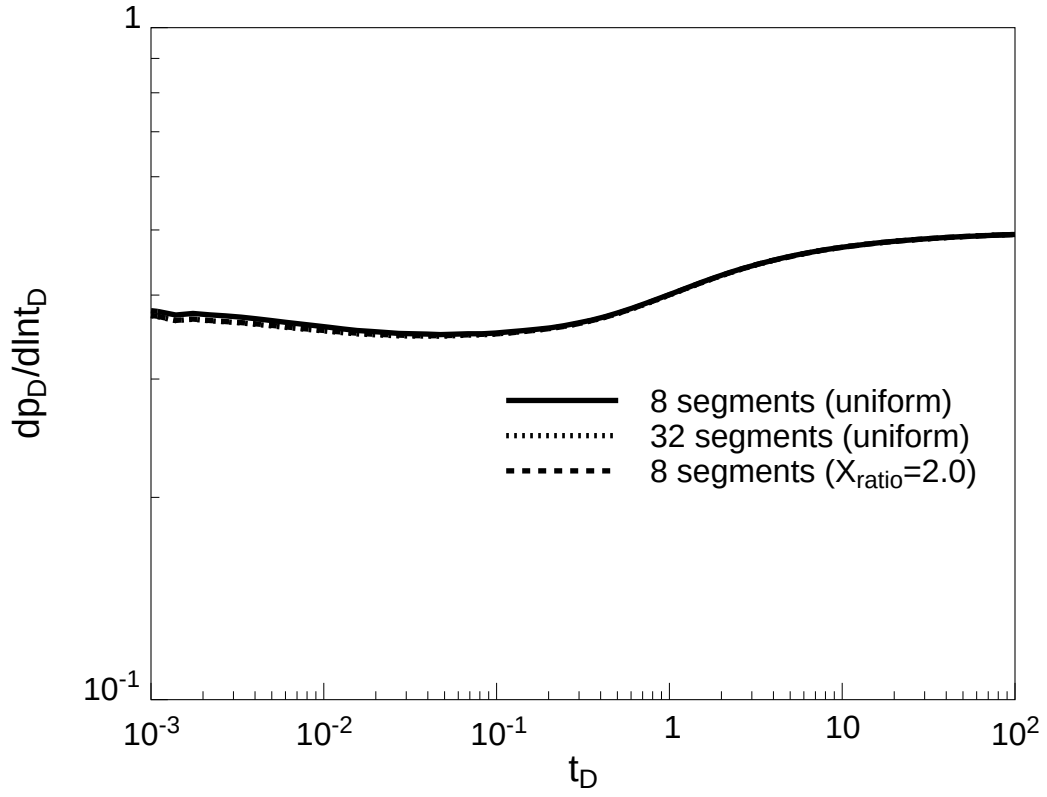

Figure 4.3: Impact of Subdivision of Segments

$X_{ratio} = 2$). As shown in Fig. 4.3, the pressure derivative of the 8-segment scheme is a little different from the result of 32-segment, if both are using uniform schemes. However, using $X_{ratio} = 2$, the pressure behavior of 8-segment scheme is almost the same as that of the fine scheme.

Gommard [17] showed that a number of 10 segments with $X_{ratio} = 2$ can give a good match of the pressure solution. Through our study, we used a number of 8 segments with $X_{ratio} = 2$ for the wellbore in each layer, although the results may be not very precise in some special cases.

4.4.2 Effect of Inclination

In highly anisotropic reservoirs ($k_v \ll k_h$), the production of slanted wells is very sensitive to the well angle if the angle is very small, i.e., $0 \leq \theta_w \leq 10^o$. If we ignored the inclination, we would obtain wrong results, especially in well test analysis.

In our study, the coordinate system was chosen in the principal directions of the permeability tensor so that $\mathbf{K}$ has three nonzero diagonal elements and zero off-diagonal elements

$$\mathbf{K} = \begin{pmatrix} k_x & 0 & 0 \\ 0 & k_y & 0 \\ 0 & 0 & k_z \end{pmatrix}. \tag{4.57}$$

For slanted wells, we set up a local coordinate system by rotating the original coordinates by angle the θ_w around the y-axis. Therefore in a plane perpendicular to the well, we have

$$k'_y = (\mathbf{K} \cdot \mathbf{e}_{\mathbf{y}'})^T \cdot \mathbf{e}_{\mathbf{y}'} = k_y \tag{4.58}$$

$$k'_z = (\mathbf{K} \cdot \mathbf{e}_{\mathbf{z}'})^T \cdot \mathbf{e}_{\mathbf{z}'} = k_z \cos^2\theta_w + k_x \sin^2\theta_w, \tag{4.59}$$

where $\mathbf{e}_{\mathbf{y}'} = [0, 1, 0]^T$ and $\mathbf{e}_{\mathbf{z}'} = [-\sin\theta_w, 0, \cos\theta_w]^T$. For horizontal wells, the production index is

$$PI = C_{we} \frac{2\pi h \sqrt{k_y k_z}}{\mu}, \tag{4.60}$$

where C_{we} is constant depending on wellbore radius. So for slanted wells, we have

$$PI' = C_{we} \frac{2\pi h \sqrt{k'_y k'_z}}{\mu} = \frac{k_z \cos^2\theta_w + k_x \sin^2\theta_w}{k_z} PI = (\cos^2\theta_w + \frac{1}{\lambda_z}\sin^2\theta_w) \cdot PI. \tag{4.61}$$

The inclination angle θ_w is very small, so we have

$$\cos^2\theta_w = \frac{1 + \cos 2\theta_w}{2} = 1 - \theta_w^2 + O(\theta_w^4), \tag{4.62}$$

$$\sin^2\theta_w = \frac{1 - \cos 2\theta_w}{2} = \theta_w^2 + O(\theta_w^4). \tag{4.63}$$

From the above equations, we have the *productivity improvement factor* (PIF) defined as

$$PIF = \frac{PI'}{PI} = (1 - \theta_w^2) + \frac{1}{\lambda_z}\theta_w^2. \tag{4.64}$$

In strongly anisotropic reservoirs, $\lambda_z = k_z/k_x$ is very small, the PIF will be very sensitive to the value of θ_w. Table 4.4.2 presents productivity improvement factors in different anisotropic reservoirs with different inclination angles.

θ_w	$\lambda_z = k_z/k_x$			
	1	0.1	0.01	0.001
0^o	1	1	1	1
3^o	1	1.025	1.27	3.74
5^o	1	1.069	1.75	8.61
10^o	1	1.274	4.02	31.4

Table 4.2: Sensitivity of Production Index to Inclination in Strongly Anisotropic Reservoirs

At first, let us consider the same reservoir as in Section 4.4.1, with a well offset of 50 ft. We investigated several different inclination angles, as shown in Fig. 4.4. The derivative curves clearly indicate the first radial flow periods before the effect of the no-flow boundaries occurs. The early-time behaviors are totally different even though the inclination only changed a little ($\Delta\theta_w \leq 5^o$). The late-time behaviors (radial flow) are very similar for all the cases, since they depend only on the hydraulic diffusivity $k_h/\phi\mu c_t$. The dimensionless pressure derivative $dp_D/d\ln t_D$ at late time can be determined by

$$\frac{dp_D}{\ln t_D} = \frac{L_w\sqrt{\lambda_z}}{h}. \tag{4.65}$$

The transition period also shows that slanted wells see boundaries much earlier than horizontal wells.

If we set the bottom boundary as constant-pressure, the early-time behaviors do not change for either of the cases (horizontal or slanted wells), as shown in Fig. 4.5. However, the transition period shows much difference between the two cases.

In multilayered reservoirs, the effect of inclination is much more complicated. First of all, the strong anisotropy plays a important role on the pressure transient behavior, especially at the early time. Secondly, the heterogeneity also makes the pressure behavior unpredictable in some cases, and it is very important to determine whether the slanted wells cross interfaces between layers.

Table 4.4 (No. 2) presents the formation properties of a two-layered reservoir,

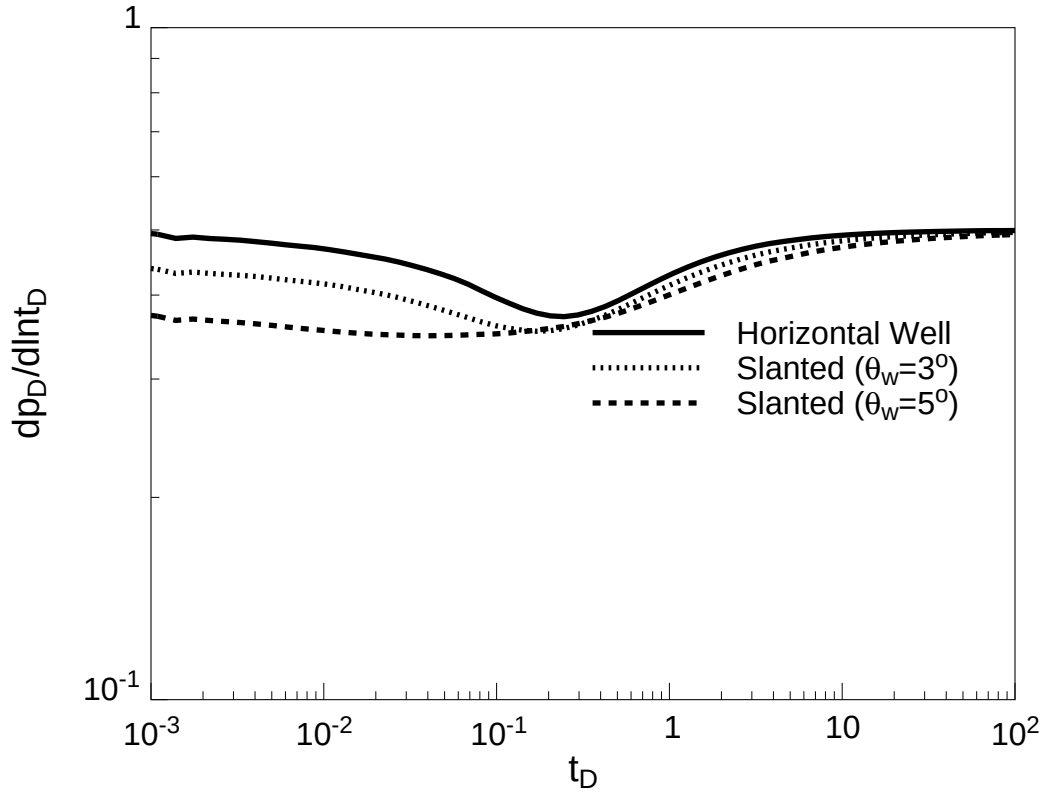

Figure 4.4: Effect of Inclination in Single-Layered Reservoirs

with which a slanted well has an offset of 10 ft. Layer 1 is the reference layer. The results are shown in Fig. 4.6. For $\theta_w = 0$ (horizontal well), the early-time pressure derivative is very high due to the low permeability of the top layer. For $\theta_w = 3^o$ and $\theta_w = 5^o$, one part of the well enters the higher-permeability bottom layer, so the pressure derivatives decrease substantially. The late time behaviors are similar for all the cases, where

$$\frac{dp_D}{\ln t_D} = \frac{L_w\sqrt{(k_h)_r(k_v)_r}}{< kh >}, \tag{4.66}$$

and

$$< kh >= \frac{\sum_{i=1}^{n}(k_h)_i h_i}{\sum_{i=1}^{n} h_i}. \tag{4.67}$$

In this case, the early radial flow of slanted wells is not very obvious due to the heterogeneity in the z-direction.

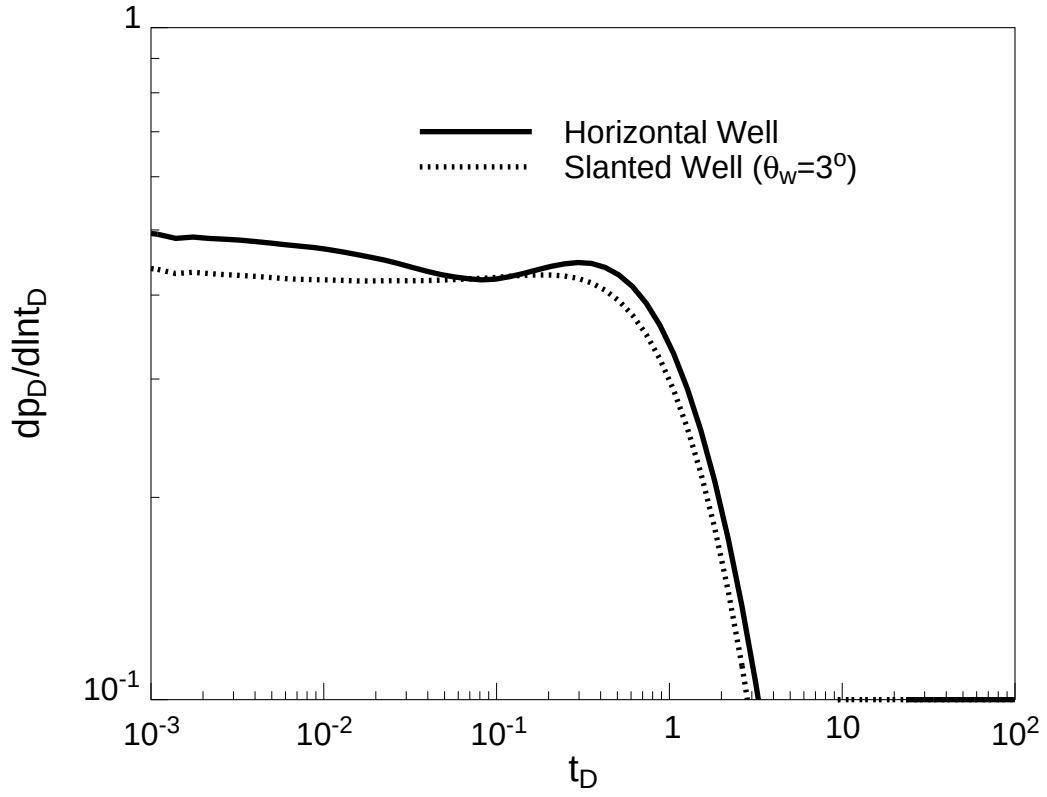

Figure 4.5: Single Layer with Constant-Pressure Bottom

4.4.3 Crossflow Between Layers

Crossflow between layers in multilayered reservoirs has a very strong impact on the pressure transient behavior. When reservoirs are strongly heterogeneous in the z-direction (the permeabilities of different layers have large differences), the communication between layers becomes crucial to the performance, otherwise the only connection is the wellbore in commingled reservoirs.

For example, we investigated the pressure response of a slanted well in a two-layered reservoir with no-flow boundaries at the top and the bottom (the formation properties are given by Table 4.4 (No. 2)), either with or without crossflow between layers. Fig. 4.7 shows that the early time pressure drop in the commingled reservoir is much higher than that of the crossflow reservoir, because the wellbore sees the boundary earlier (interfaces between layers become no-flow boundaries in commingled reservoirs). The transition periods are also totally different. Therefore, we can not

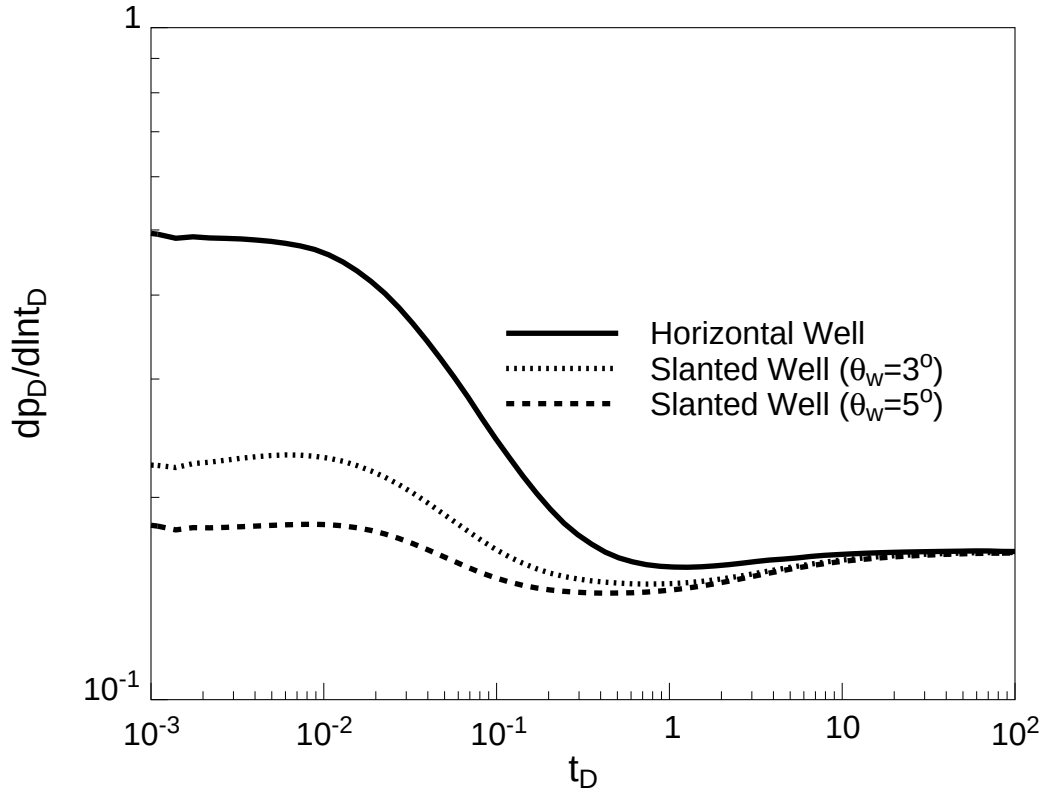

Figure 4.6: Effect of Inclination in Two-Layered Reservoirs

treat crossflow reservoirs as commingled reservoirs.

4.4.4 Effect of Layer Thickness

It is very import to determine the thickness of all layers in multilayered reservoirs very precisely, otherwise we may jump to a wrong conclusion. The following example shows that the thickness of the layers affects the pressure behavior significantly, even though the formation properties of the layers and the total thickness are unchanged.

This example is a three-layered reservoir, the formation properties are shown in Table 4.4 (No. 3). Fig. 4.8 clearly shows the difference between two situations, although we only change the thickness a little ($\Delta h_i \leq 10$ft).

We also examined a six-layered system, whose formation properties are given by Table 4.4 (No. 4). Fig. 4.9 shows the pressure derivatives for such a complicated

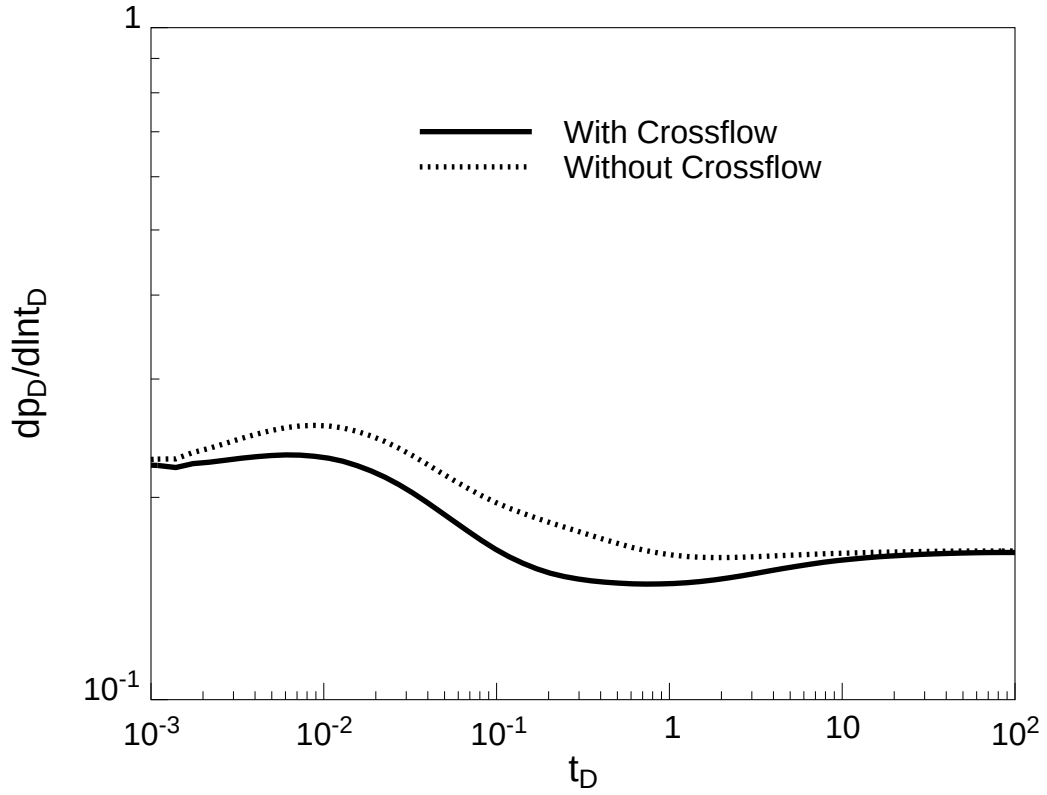

Figure 4.7: Effect of Crossflow in Multilayered Reservoirs

reservoir. In practice, the identification of such a layered system may not be possible and may also lead us to an incorrect interpretation. As we showed before, the pressure responses are very sensitive to thickness of the layers, so if the number of layers is large, it will be very difficult to determine the thickness and the properties of each layer very precisely.

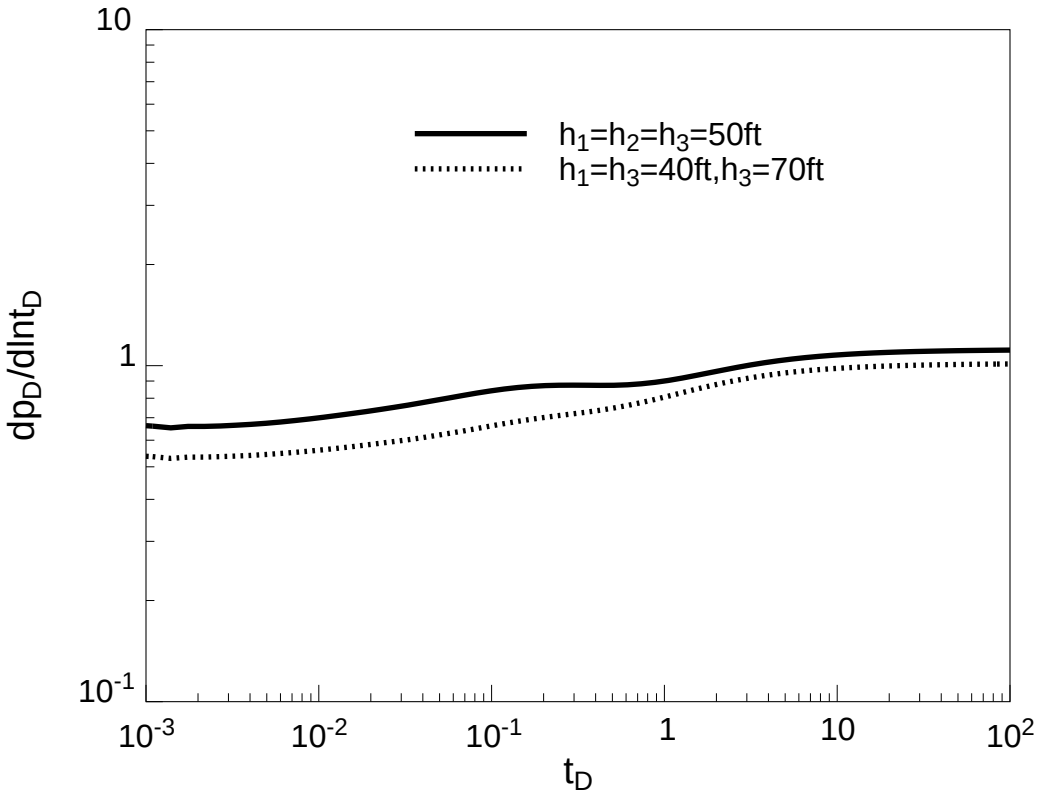

Figure 4.8: Effect of Thickness of Layers

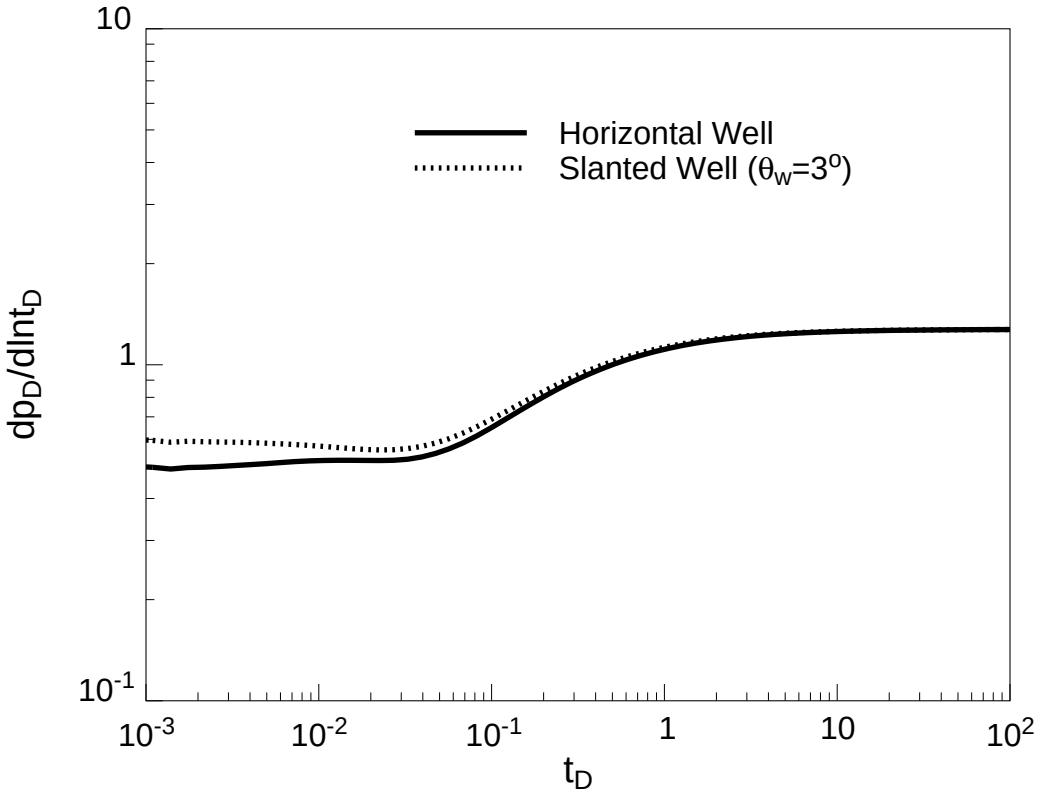

Figure 4.9: A Six-Layered System

Section 5

Interference between Horizontal Wells

5.1 Problem Description

It is not uncommon that there are several horizontal wells completed in a layered reservoir, in which case the interference between the wells becomes very important, especially at the late time. In this section, we study the interference between the horizontal wells in layered reservoirs.

The configuration of the layered reservoir is the same as described in Section 4.1. There are several horizontal wells located in different layers, with arbitrary locations and orientations, as shown in Fig. 5.1. The center of Well i is located at point (x_i, y_i, z_i), the orientation (deviation from x-axis) is θ_i. Each layer is assumed to be horizontally isotropic, so $k_x = k_y$.

5.2 Segmentation Technique for Multiwell Systems

The basic construction of the linear equation for pressure drop and flow rate is almost the same as defined in Section 4.2, but there are some difference because there are more than one wellbore in this system. We derive the linear equation in the Laplace space as follows.

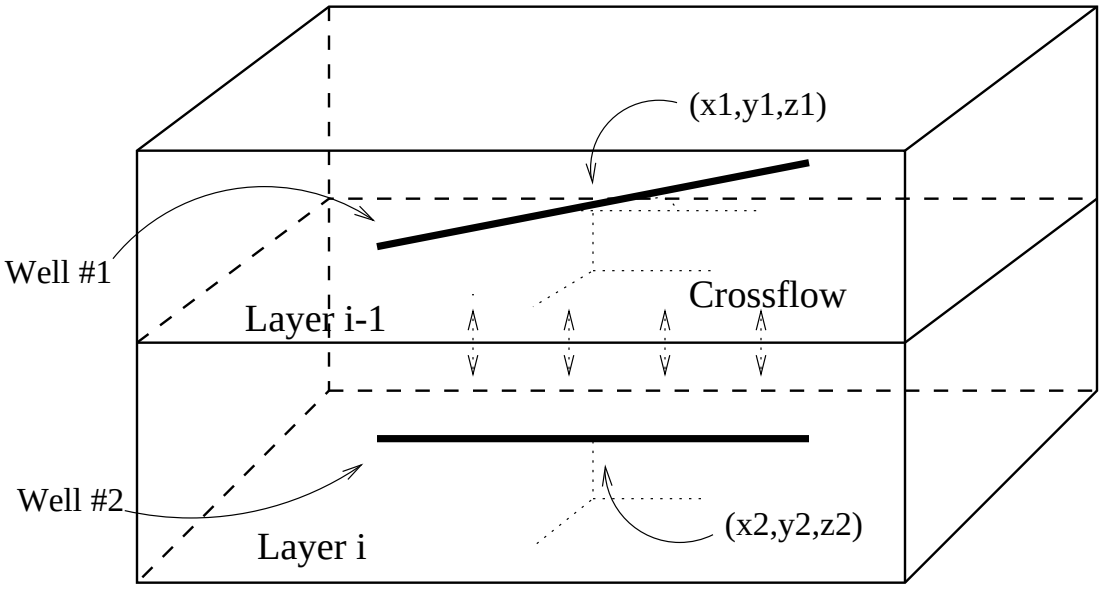

Figure 5.1: Configuration of Multiwell Reservoir

The infinite-conductivity constraint yields

$$\Delta\bar{p}_i^{(j)}(s) = \Delta\bar{p}_i(s) \;\; j = 1, 2, \ldots, N_i, \tag{5.1}$$

and the flow constraint yields

$$\sum_{j=1}^{N_i} l_i^{(j)} \cdot \bar{q}_i^{(j)}(s) = Q_i/s, \tag{5.2}$$

for $i = 1, \ldots, n$, and n is the number of the wells in the reservoir, and N_i denotes the number of segments in Well i. In Eqs. 5.1 and 5.2, the denotation $v_i^{(j)}$ represents the value of v on j-th segment of Well i and v_i represents the value of v of Well i.

The linear relations between flow rates and pressure drops are given as

$$\Delta\bar{p}_i^{(j)}(s) = \sum_{k=1}^{n} \sum_{l=1}^{N_k} \bar{G}_{i^{(j)},k^{(l)}}(s) \cdot \bar{q}_k^{(l)}(s), \tag{5.3}$$

where $i^{(j)}$ denotes the overall index of Segment j of Well i.

Combining Eqs. 5.1, 5.2 and 5.3, we have a linear equation for $\bar{p}_i(s)$ and $\bar{q}_i^{(j)}(s)$ as

$$\begin{bmatrix} G_{N\times N} & -J_{N\times n} \\ L_{n\times N} & 0_{n\times n} \end{bmatrix} \cdot \begin{bmatrix} \bar{\mathbf{q}}_N \\ \Delta\bar{\mathbf{p}}_n \end{bmatrix} = \begin{bmatrix} \mathbf{0}_N \\ \mathbf{Q}_n/s \end{bmatrix}, \tag{5.4}$$

where

$$J_{i^{(j)},i} = 1 \tag{5.5}$$

$$L_{i,i^{(j)}} = l_i^{(j)} \tag{5.6}$$

other elements in J and L are all zeros.

Solving Eq. 5.4 yields

$$\Delta\bar{\mathbf{p}} = (LG^{-1}J)^{-1} \cdot \mathbf{Q}/s \tag{5.7}$$

$$\bar{\mathbf{q}} = G^{-1}J \cdot \Delta\bar{\mathbf{p}}, \tag{5.8}$$

then we used the same technique presented in Section 4.2 to calculate them.

5.3 Green's Functions for Segments

The construction of the Green's Functions of segments in this part is only a special case with the inclined angle $\theta_w = 0$. However, because the vertical offsets of the wells are constants, we obtained a much simpler form, which can speed up the calculations. In this case, the homogeneous solutions are only functions of α and β, so we have

$$\begin{aligned} < \bar{G}_h(s, \mathbf{r}, \mathbf{r_j}) >_i = & \frac{4}{\pi^2} \int_{L_i} dl \cdot \int_0^\infty \int_0^\infty d\alpha d\beta \\ & \cdot \bar{\bar{G}}_h(s, \alpha, \beta, z_i; z_j) \cos(\alpha(x - x_j)) \cos(\beta(y - y_j)). \end{aligned} \tag{5.9}$$

Since the medium is horizontally isotropic, we can rotate the coordinates around the z-axis at will. In order to simplify the calculation, we set Well $w(i)$ parallel to the x-axis, where $w(i)$ denotes the well index of Segment i, i.e., Segment i is at Well $w(i)$. Thus we have

$$(x_j, y_j) \to (x'_j, y'_j), \tag{5.10}$$

and

$$(x, y) \to (x', 0) \text{ on Well } w(i), \tag{5.11}$$

so

$$\begin{aligned} < \bar{G}_h(s, \mathbf{r}, \mathbf{r_j}) >_i = &= \frac{4}{\pi^2} \int_0^\infty \int_0^\infty d\alpha d\beta \\ &\cdot \bar{\bar{G}}_h(s, \alpha, \beta, z_i; z_j) \int_{-l_i/2}^{l_i/2} dx \cos(\alpha(x' - x'_j)) \cos(\beta y'_j) \\ &= \frac{4}{\pi^2} \int_0^\infty \int_0^\infty d\alpha d\beta \cdot \bar{\bar{G}}_h(s, \alpha, \beta, z_i; z_j) S(s, \alpha, \beta), \end{aligned} \tag{5.12}$$

where

$$\begin{aligned} S(s, \alpha, \beta) &= \int_{-l_i/2}^{l_i/2} dx \cos(\alpha(x' - x'_j)) \cos(\beta y'_j) \\ &= \frac{\sin \alpha(x' - x'_j)}{\alpha} \cos \beta y'_j \; |_{-l_i/2}^{l_i/2} \\ &= 2 \frac{\sin \frac{\alpha l_i}{2} \cos \alpha x_j \cos \beta y'_j}{\alpha}. \end{aligned} \tag{5.13}$$

5.4 Results and Discussion

At first, we investigated the impact of crossflow between layers. A two-layered reservoir is considered here, and the reservoir formation properties are given by Table 5.4, which is the same as in Table 4.4 (No. 2). Two horizontal wells are located in different layers in this reservoir. As shown in Fig. 5.2, in commingled reservoirs, the interfaces between layers are treated as no-flow boundaries, so interference between horizontal wells doesn't exist. Each well behaves as a single well in a homogeneous reservoir. However, in crossflow reservoirs, the communication between layers makes the late time behavior (pressure derivative) very similar for all horizontal wells in the reservoir, although it may take a very long time to reach that radial flow period. Therefore, in commingled reservoirs, we can solve each layer independently. In crossflow reservoirs, the situation will be much more complicated, interference between the horizontal wells plays a very important role, especially in the transition and late time periods.

Layer	$h(ft)$	$k_h(md)$	$k_v(md)$
1(r)	100	100	1
2	100	200	10

Table 5.1: Reservoir Parameters for a Multiwell Reservoir

The orientation of the horizontal wells can also affect their pressure transient behaviors in such a situation. Fig. 5.3 shows the effect of orientation. The configuration of the reservoir is the same as in the previous example. In this example, we investigated the pressure response in two different configurations, one with two parallel horizontal wells, another with two perpendicular horizontal wells, while the locations of wells and distances between the centers of wells are the same. Fig. 5.3 shows that the transition period is modestly dependent on the orientation of wells, although the early and late time periods are not sensitive.

If the distances between the horizontal wells are very large, the interference in the early time and transition periods may be trivial. In this case, the pressure transient response may show some characteristics of radial flow behavior in the transition period (flat lines in pressure derivative curves), then a late-time radial flow regime may appear at very late time. Just as shown in Fig. 5.4, when the distance between Well #1 and Well #2 is very large ($\Delta y = 10000\,ft$), each well shows its individual early-time and transition-period response, then the wellbore sees the boundaries before it see the other wells, so it shows a radial flow behavior. After a very long time (beyond the time scale of Fig. 5.4), both the wells show a similar late-time behavior in pressure derivative diagram.

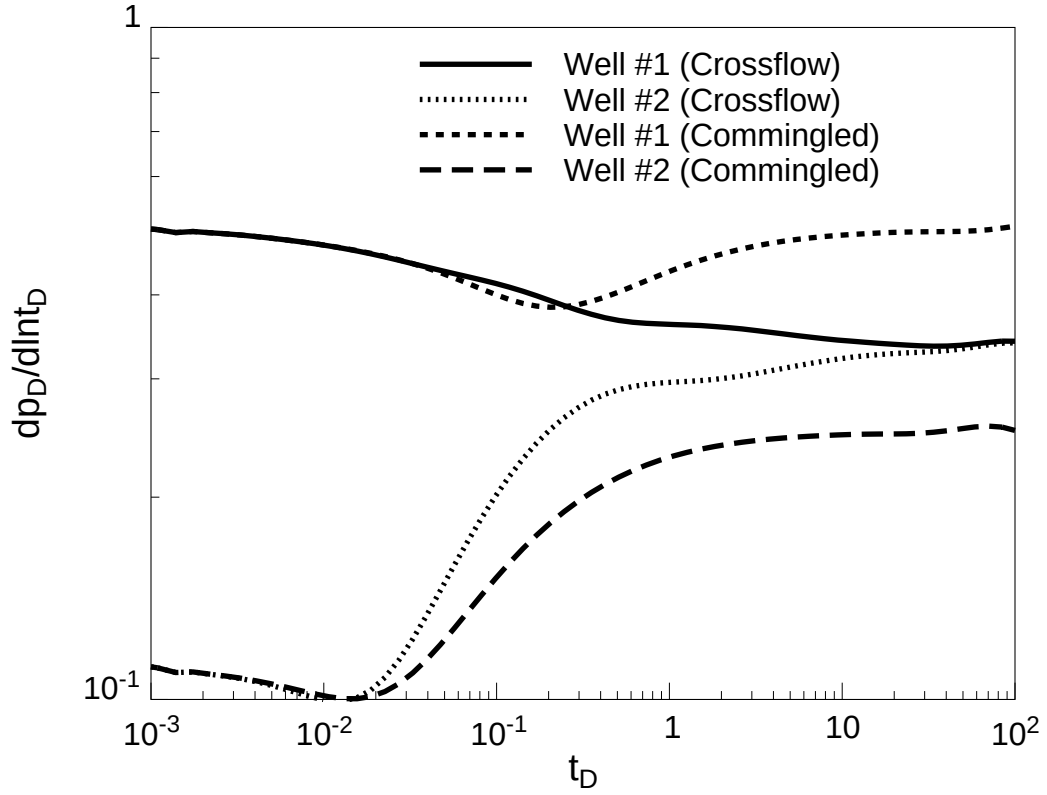

Figure 5.2: Effect of Crossflow for Interference

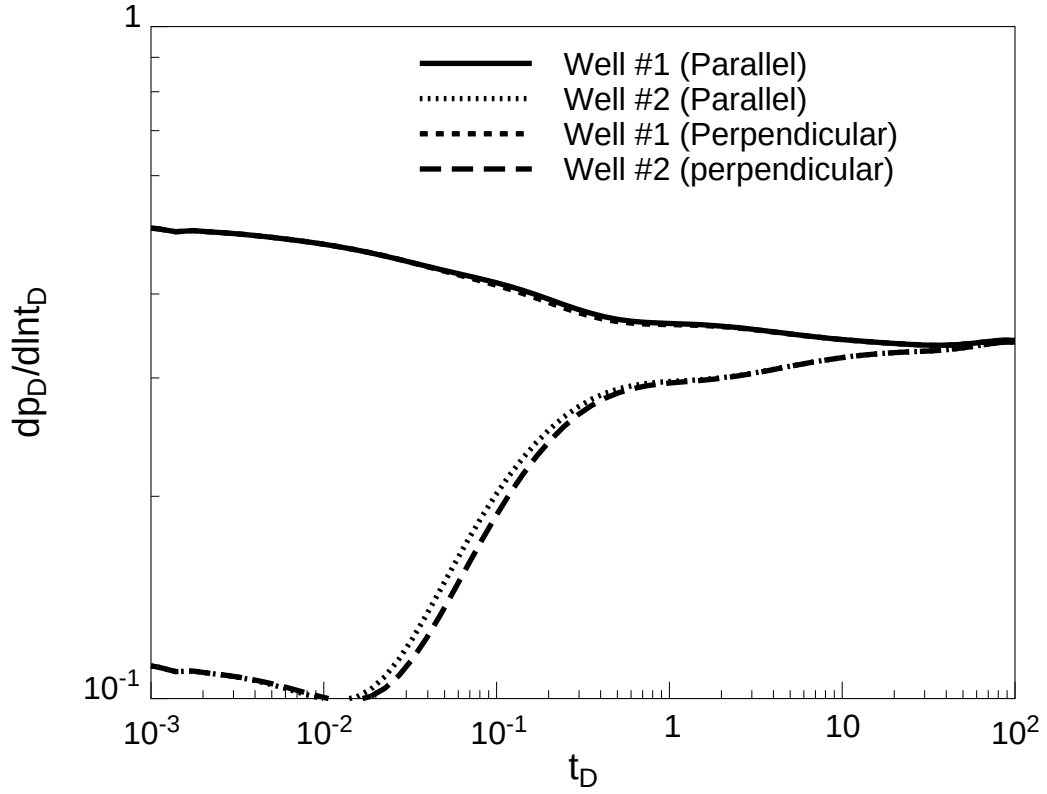

Figure 5.3: Effect of Crossflow for Interference

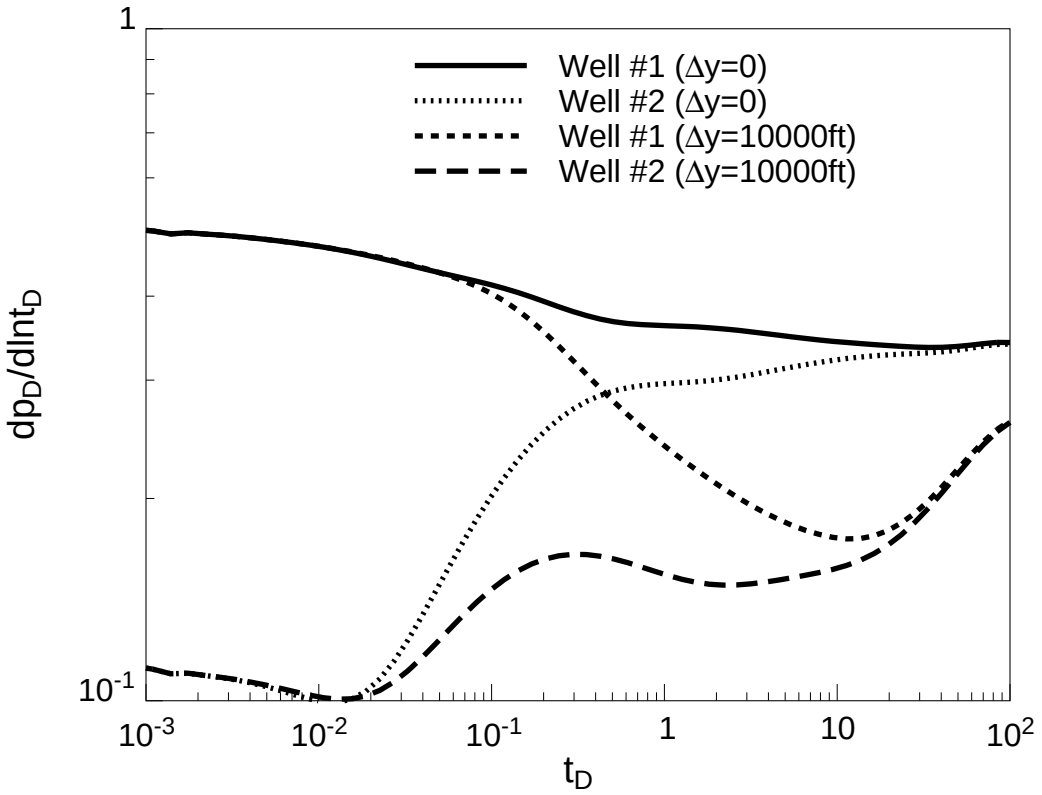

Figure 5.4: Effect of Distance between Wells

Section 6

Conclusions and Future Work

6.1 Conclusions

In this study, we developed new analytical solutions to describe the pressure-transient behaviors of slanted and horizontal wells in multilayered reservoirs. We applied the Laplace transformation and the Fourier transformation to generate the Green's functions for layered and composite reservoirs. An algorithm to compute the solutions in such complicated situations was also developed. The validation and efficiency of this algorithm were investigated in two different projects: slanted wells crossing layers and interference between horizontal wells in multilayered reservoirs with crossflow. From the application examples, we can make the following conclusions:

1. The algorithm is practical in obtaining precise and reliable solutions analytically. The solution is valid for a wide range of configurations of reservoirs.

2. In strongly anisotropic layered reservoirs, slanted wells can produce more effectively than horizontal and vertical wells. Therefore, the inclinations of wells can not be ignored in such situations. The early time behavior is very important to determine the properties of the formation. Consequently, well test analysis is more difficult because the early time pressure responses are not available in many situations.

3. Due to interference between horizontal wells, the transition period of multiwell systems becomes very complicated. Therefore it is very difficult for us to identify the pressure-transient behavior of an individual well. Furthermore, because the overall pressure response is sensitive to the locations and orientations of all the wells in the reservoir, the determination of well locations and thickness of layers becomes crucial.

4. In both cases, the crossflow between layers can not be ignored, otherwise, we may obtain incorrect results. The effect of crossflow play a very important role in layered reservoirs.

6.2 Future Work

For a slanted well in a multilayered reservoir, because the wellbore crosses many layers with different properties, the skin factor of the wellbore may depend on these properties. In different flow regimes, the flux distribution along the wellbore will also change, so the skin factor is not a constant. It will be necessary to determine a time-dependent skin factor.

Although the algorithm developed in our study is very efficient, it is not fast enough for use in nonlinear regression (it takes up to two or three minutes to generate a solution on a DEC workstation). Therefore, a more efficient algorithm will be necessary.

Nomenclature

c_t	Total isothermal compressibility
G	Green's function
h	Formation thickness
k_x	Permeability
l	Segment length
L_w	Half wellbore length
n	Outward normal
p	Pressure
p_D	Dimensionless pressure
q	Flow rate
Q	Total flow rate
$\mathbf{r}$	Position vector
r_w	Wellbore radius
R	Local reflection coefficient
R_U	Upgoing global reflection coefficient
R_D	Downgoing global reflection coefficient
s	Parameter of Laplace transformation
S	Skin factor
t	Time
T	Local transmission coefficient

GREEKS

α,β	Parameters of double Fourier transformation
$\delta(x, x')$	Dirac delta function
ϕ	Porosity
μ	Fluid viscosity
γ	Boundary constant
ζ	Boundary constant
θ_w	Inclination angle
λ	Permeability ratio
κ	
η	
Ω	Domain of the problem domain
Γ	Boundary of the problem domain

SUBSCRIPTS

0	Initial
D	Dimensionless
i, j, l	Integer indices
r	Reference

SUPSCRIPTS

-	Laplace transformed variable
=	Double Fourier transformed variable

Bibliography

[1] Goode, P.A. and Thambynayagam, R.K.M.: "Pressure Drawdown and Buildup Analysis of Horizontal Wells in Anisotropic Media," SPEFE (Dec. 1987) 683-97; Trans., AIME, 283.

[2] Kuchuk, F.J.: "Well Testing and Interpretation for Horizontal Wells," JPT (January 1995) 36-40.

[3] Rosa, Adalberto J., and Carvalho, R. de S.: "A Mathematical Model for Pressure Evaluation in an Infinite-Conductivity Horizontal Well ," SPEFE (Dec. 1989) 559-566.

[4] Ozkan, E., Raghavan, R. and Joshl, S.D.: "Horizontal-Well Pressure Analysis," SPEFE (Dec. 1989) 567-575.

[5] Odeh, A.S. and Babu, D.K.: "Transient Flow Behavior of Horizontal Wells: Pressure Drawdown and Buildup Analysis," SPEFE (March 1990) 7-15.

[6] Kuchuk F.J., Goode, P.A., Brice, B.W., Sherrard, D.W. and Thambynayagam, R.K.M.: "Pressure-Transient Analysis for Horizontal Wells ," JPT (August 1990) 974-979.

[7] Kuchuk, F.J., Goode, P.A., Wilkinson, D.J. and Thambynayagam, R.K.M.: "Pressure-Transient Behavior of Horizontal Wells with and Without Gas Gap or Aquifer," SPEFE (March 1991) 68-94.

[8] Kuchuk, F.J. and Habashy, T.: "Pressure Behavior of Linear and Radial Composite Systems," Schlumberger-Doll Research report, Ridgefield, CT (1991).

[9] Spath, J.B., Ozkan, E. and Raghavan, R.: "An Efficient Algorithm for Computation of Well Responses in Commingled Resvervoirs," SPEFE (June 1994) 115-121.

[10] Kuchuk, F.J.: "Pressure Behavior of Horizontal Wells in Multilayer Reservoirs With Crossflow," SPE 22731 presented at the 66th SPE Annual Technical Conference and Exhibition, Dallas, TX (1991).

[11] Kuchuk, F.J.: "Pressure Behavior of Laterally Composite Reservoirs," SPE 24678 presented at the 67th SPE Annual Technical Conference and Exhibition, Washington, DC (1992).

[12] Roemershauser, A.E. and Hawkins, M.F., Jr.: "The Effect of Slant of a Slant Hole, Drainhole, and Lateral Hole Drilling on a Well Productivity," JPT (Feb. 1955) 11-14.

[13] Cinco, H.: "Unsteady-State Pressure Distributions Created by a Slanted Well or a Well in an Inclined Fracture," PhD dissertation, Stanford U., Stanford, Calif. (1974).

[14] Cinco, H., Miller, F.G. and Ramey, H.J.: "Unsteady-State Pressure Distribution Created by a Directionally Drilled Well," Trans., AIME (1975) 259, 1392-1400.

[15] Fair, P.S., Kikani, J. and White, C.D.: "Modeling High Angle Wells in Laminated Reservoirs," SPE 36728 presented at the 71th SPE Annual Technical Conference and Exhibition, Denver, CO (1996).

[16] Lee, S.H. and Milliken, W.J.: "The Productivity Index of an Inclined Well in Finite-Difference Reservoir Simulation," SPE 25247 presented at the 12th SPE Symposium on Reservoir Simulation, New Orleans, LA (1993).

[17] Gommard, Denis: "Computing the Solution for Almost Horizontal Wells," SUPRI-D report, Stanford U., Stanford, CA (1996).

[18] Gringarten, A.C. and Ramey, Jr. H.J.: "The Use of Source and Green's Functions in Solving Unsteady-Flow Problems in Reservoirs," SPE 3818 (1973).

[19] Kong, J.A. (ed.): "Research Topics in Electromagnetic Wave Theory," John Wiley & Sons, New York (1981).

[20] Wilkinson, D. and Hammond, P.S.: "A Perturbation Method for Mixed Boundary Value Problems in Pressure Transient Testing," Transport in Porous Media (1990) 5, 609-636.

[21] van Everdingen, A.F. and Hurst, W.: "The Application of Laplace Transformation to Flow Problems in Reservoirs," Trans., AIME (1949) 186, 305-324.

[22] Agarwal, G.R., Al-Hussainy, R., and Ramey, H.J. Jr.: " An Investigation of Wellbore Storage and Skin Effect In Unsteady Liquid Flow: I. Analytical Treatment," Trans. AIME (1970) 249, 279-290.

[23] Stehfest, H.: "Numerical Inversion of Laplace Transforms," Communications ACM, 13 No. 1 (1970) 47-49.

[24] Ozkan, E.: "Some Strategies to Exploit the Laplace Transformation for a Tabulated Set of Numbers," SPE 30552 presented at the 70th SPE Annual Technical Conference and Exhibition, Dallas, TX (1995).

Computer Programs